NAT'L INST. OF STAND & TECH R.I.C.
A11104 577148
NIST
PUBLICATIONS

NISTIR 5608

Electronics and Electrical Engineering Laboratory

J. M. Rohrbaugh
Compiler

Technical Progress Bulletin

94-4

Covering Laboratory Programs,
October to December 1994
with 1995 EEEL Events Calendar

U.S. DEPARTMENT OF COMMERCE
Technology Administration
National Institute of Standards
and Technology

NIST

QC
100
.U56
NO.5608
1995

NISTIR 5608

Electronics and Electrical Engineering Laboratory

J. M. Rohrbaugh
Compiler

Electronics and Electrical
Engineering Laboratory
Semiconductor Electronics Division
Gaithersburg, MD 20899

Technical Progress Bulletin

March 1995

94-4

Covering Laboratory Programs,
October to December 1994
with 1995 EEEL Events Calendar

U.S. DEPARTMENT OF COMMERCE
Ronald H. Brown, Secretary
TECHNOLOGY ADMINISTRATION
Mary L. Good, Under Secretary for
Technology
NATIONAL INSTITUTE OF STANDARDS
AND TECHNOLOGY
Arati Prabhakar, Director

ELECTRONICS AND ELECTRICAL ENGINEERING LABORATORY
TECHNICAL PROGRESS BULLETIN, MARCH 1995 ISSUE

INTRODUCTION

This is the forty-ninth issue of a quarterly publication providing information on the technical work of the National Institute of Standards and Technology Electronics and Electrical Engineering Laboratory (EEEL). This issue of the EEEL Technical Progress Bulletin covers the fourth quarter of calendar year 1994.

Organization of Bulletin: This issue contains abstracts for all relevant papers released for publication by NIST in the quarter and citations and abstracts for such papers published in the quarter. Entries are arranged by technical topic as identified in the Table of Contents and alphabetically by first author under each subheading within each topic. Unpublished papers appear under the subheading "Released for Publication." This does not imply acceptance by any outside organization. Papers published in the quarter appear under the subheading "Recently Published." Following each abstract is the name and telephone number of the individual to contact for more information on the topic (usually the first author). This issue also includes a calendar of Laboratory conferences and workshops planned for calendar years 1995 and a list of sponsors of the work.

Electronics and Electrical Engineering Laboratory: EEEL programs provide national reference standards, measurement methods, supporting theory and data, and traceability to national standards. The metrological products of these programs aid economic growth by promoting equity and efficiency in the marketplace, by removing metrological barriers to improved productivity and innovation, by increasing U.S. competitiveness in international markets through facilitation of compliance with international agreements, and by providing technical bases for the development of voluntary standards for domestic and international trade. These metrological products also aid in the development of rational regulatory policy and promote efficient functioning of technical programs of the Government.

The work of the Laboratory is conducted by five technical research Divisions: the Semiconductor Electronics and the Electricity Divisions in Gaithersburg, Md., and the Electromagnetic Fields and the Electromagnetic Technology Divisions, and the newly formed Optoelectronics Division in Boulder, Colo. The Office of Law Enforcement Standards conducts research and provides technical services to the U.S. Department of Justice and State and local governments, and other agencies in support of law enforcement activities. In addition, the Office of Microelectronics Programs (OMP) coordinates the growing number of semiconductor-related research activities at NIST. Reports of work funded through the OMP are included under the heading "Semiconductor Microelectronics."

Key contacts in the Laboratory are listed at the end of this publication; readers are encouraged to contact any of these individuals for further information. To request a subscription or for more information on the Bulletin, write to EEEL Technical Progress Bulletin, National Institute of Standards and Technology, Metrology Building, Room B-358, Gaithersburg, MD 20899 or call (301) 975-2220.

Laboratory Sponsors: The Laboratory Programs are sponsored by the National Institute of Standards and Technology and a number of other organizations, in both the Federal and private sectors; these are identified on page 44.

Note on Publication Lists: Publication lists covering the work of each division are guides to earlier as well as recent work. These lists are revised and reissued on an approximately annual basis and are available from the originating division. The current set is identified in the Additional Information section, page 40.

Certain commercial equipment, instruments, or materials are identified in this paper in order to specify adequately the experimental procedures. Such identification does not imply recommendation or endorsement by the National Institute of Standards and Technology, nor does it imply that the materials or equipment identified are necessarily the best available for the purpose.

TABLE OF CONTENTS

NATIONAL SEMICONDUCTOR METROLOGY PROGRAM ESTABLISHED

The semiconductor industry has strongly urged the Administration and Congress to establish a major metrology program at NIST, and in March 1994, the resulting National Semiconductor Metrology Program was announced. Program funding is planned to ramp up over several years to a final level of $25 million per year. Industry's backing resulted from the record of useful solutions from NIST coupled with an increasing appreciation on the part of industry leaders of the key role of metrology in advanced competitive products. This program reinforces NIST's role as the nation's lead laboratory for metrology and exemplifies NIST's charter to serve industry. [Contact: Robert I. Scace, (301) 975-2485]

FUNDAMENTAL ELECTRICAL MEASUREMENTS

Released for Publication

Benz, S.P., Reintsema, C.D., Ono, R.H., Eckstein, J.N., Bozovic, I., and Virship, G.F., **Step-Edge and Stacked-Heterostructure High-T_c Josephson Junctions for Voltage Standard Arrays**.

[See Cryoelectronic Metrology.]

Clark, A.F., Zimmerman, N.M., Williams, E.R., Amar, A., Song, D., Wellstood, F., Lobb, C.J., and Soulen, R.J., **An Application of Single Electron Tunneling: Capacitance Bridge Measurement**.

We report on a demonstration of a useful application of single electron tunneling (SET) phenomena: a precision measurement of the ratio of two cryogenic capacitors. This is accomplished by using a SET electrometer as the null detector for a capacitance-bridge measurement. We have achieved a few parts per million level of precision in the measurement of capacitance ratio at 100 to 1000 Hz and suggest further improvements to be made to obtain a precision of 10^{-8} at lower frequencies; this will be necessary for the metrological measurement of capacitance or the fine-structure constant, using a SET pump.
[Contact: Alan F. Clark, (301) 975-2139]

FUNDAMENTAL ELECTRICAL MEASUREMENTS

Recently Published

Early, E.A., Steiner, R.L., Clark, A.F., and Char, K., **Evidence for Parallel Junctions within High-T_c Grain-Boundary Junctions**, Physical Review B, Vol. 50, No. 13, pp. 9409-9418 (October 1, 1994).

Half-integral constant voltage steps were observed in many high-T_c grain-boundary Josephson junctions of $YBa_2Cu_3O_{7-\delta}$ when a microwave field was applied. Five distinct observed behaviors of the widths of both integral and half-integral steps as a function of microwave amplitude, $\Delta I_{dc}(I_{ac})$, are reproduced by simulations of two or three junctions in parallel. This provides quantitative evidence that a single high-T_c grain-boundary junction is composed of several junctions in parallel. These junctions are formed by the overlap of superconducting filaments on either side of the grain boundary, and the spacing between ones with relatively large critical currents is $\sim 20\ \mu$m.
[Contact: Edward A. Early, (301) 975-4228]

Kautz, R.L., **Quasipotential and the Stability of Phase Lock in Nonhysteretic Josephson Junctions**, Journal of Applied Physics, Vol. 76, No. 9, pp. 5538-5544 (November 1994).

The principle of minimum available noise energy is used to calculate the quasipotential over the state space of a nonhysteretic Josephson junction driven by an rf bias. This potential surface provides an intuitive picture of the dynamics of phase lock and defines a stability parameter, the activation energy for thermally induced phase slippage, that determines the optimum operating conditions for a proposed programmable voltage standard.
[Contact: Richard L. Kautz, (303) 497-3391]

Kautz, R.L., Benz, S.P., and Reintsema, C.D.,

Large-Amplitude Shapiro Steps and Self-Field Effects in High-T_c Josephson Weak Links, Applied Physics Letters, Vol. 65, No. 11, pp. 1445-1447 (September 1994).

We demonstrate contiguous Shapiro steps of orders 0 and 1 having amplitudes of 1 mA in a $YBa_2Cu_3O_{7-\delta}$ step-edge junction operated at 38 K. A wide-junction model that includes self-field effects explains why the observed step amplitudes are smaller than expected from the resistively shunted point-junction model. In spite of their reduced amplitudes, the observed steps are suitable for use in a proposed rapidly programmable Josephson voltage standard.
[Contact: Richard L. Kautz, (303) 497-3391]

Lee, K.C., and Cage, M.E., **Design Challenges of a Commercial QHE-Based Resistance Standard**, NISTIR 5533 (December 1994).

Of the electrical measurements that underpin the broad spectrum of modern industry, measurements of voltage, resistance, and impedance are among the most important. National Standards Laboratories have developed intrinsic standards based on quantum effects, such as Josephson's effect and the quantum Hall effect, that can be used to realize standards of voltage and resistance with relative uncertainties approaching parts in 10^9. The equipment necessary to observe these phenomena is very complex and expensive, and these standards have not yet found wide application in industrial laboratories. This paper assesses the possibility of developing a commercially viable quantum Hall effect-based resistance standards system. The capabilities of resistance calibration systems currently in use are summarized, and specifications for a competitive quantum Hall effect-based system are described. The realization of such a system presents numerous challenges, from making suitable samples, to developing high-accuracy, automated measurement systems, to developing low-cost, reliable cryogenic systems. These technical challenges are discussed in detail, and several possible commercial systems are described.
[Contact: Kevin C. Lee, (301) 975-4236]

Williams, E.R., Olsen, P.T., and Jones, G., Jr., **Monitoring and Replacing of the Kilogram Using an Si Watt Experiment**, Proceedings of the XXIVth URSI General Assembly, Kyoto, Japan, August 25—September 2, 1993, Abstract A5-8 of the International Union of Radio Science.

By international agreement, the Josephson frequency-to-voltage quotient (or Josephson constant) and the quantum Hall resistance (or von Klitzing constant) are fixed in value. These two stable sources provide highly reproducible laboratory units of voltage and resistance which can be converted into a highly reproducible unit of electrical power. Through the use of watt balance, the stability of the mass of the kilogram can be evaluated at the accuracy of the watt determinations. It has been reported that the mass of the kilogram is thought to be stable to at least 0.01 parts per million/year. Thus, the measurement uncertainty of the watt-balance experiment would have to be of the order of 0.01 parts per million to be of significance in monitoring the stability of the international standard of mass, the SI kilogram.
[Contact: Edwin R. Williams, (301) 975-4206]

SEMICONDUCTOR MICROELECTRONICS

Compound Materials

Released for Publication

Kim, J.S., Seiler, D.G., Colombo, L., and Chen, M.C., **Characterization of Liquid-Phase Epitaxially Grown HgCdTe Films by Magnetoresistance Measurements**.

[See Analysis and Characterization Techniques.]

Pellegrino, J.G., Richter, C.A., Dura, J.A., Qadri, S.B., Roughani, B., and Amirtharaj, P.M., **Buffer Layer-MODFET Interactions in the $Al_{0.33}Ga_{0.67}As$/GaAs Superlattice System**.

The correlation between the structural and transport properties for a series of high-quality modulation-doped field-effect transistor (MODFET) structures was made for various growth temperatures. X-ray reflectivity, X-ray diffraction, and magnetotransport measurements were used to assess structural quality and transport parameters. Four samples with growth temperatures in the range 500 °C to 630 °C were examined. The results indicate a

correlation exists between the measured electron mobility and the quality of the interface width, as measured from satellite peaks of the buffer layer. Both X-ray and transport results suggest a higher quality structure was obtained at higher growth temperatures.
[Contact: Joseph G. Pellegrino, (301) 975-2123]

Compound Materials

Recently Published

Kim, J.S., Seiler, D.G., Colombo, L., and Chen, M.C., **Electrical Characterization of Liquid-Phase Epitaxially Grown Single-Crystal Films of Mercury Cadmium Telluride by Variable Magnetic-Field Hall Measurements**, Semiconductor Science and Technology, Vol. 9, pp. 1696-1705 (1994).

We report a method for a new classification procedure for liquid-phase epitaxially grown mercury-cadmium-telluride single crystals. Variable-magnetic-field Hall measurements are performed on nine liquid-phase epitaxially grown $Hg_{0.78}Cd_{0.22}Te$ single-crystal films for magnetic fields from 0 to 1.4 T and in the temperature range from 10 K to 300 K. The data from these measurements are analyzed in the context of the reduced-conductivity-tensor scheme proposed by Kim and coworkers. Based on the degree of deviation from an ideal one-carrier behavior, these experimental samples are classified into several types to emphasize the transition in the behavior of the normal to anomalous n-type samples, finally leading to p-type samples. Our classification is also based on a general trend in the temperature dependence of the mobility and density of the majority carriers which were extracted from the magnetoresistivity data. The classification provides a useful benchmark for materials characterization in the infrared detector industry.
[Contact: Jin S. Kim, (301) 975-2238]

Lowney, J.R., Kim, J.S., and Seiler, D.G., **Magnetotransport Properties of HgCdTe**, EMIS Data Review, in Properties of Narrow Gap Cadmium-Based Compounds, Chapter A6.12, P. Capper, Ed. (INSPEC, London, 1994), pp. 264-270.

Magnetotransport techniques are widely used to characterize the electrical properties of HgCdTe. The Hall-effect method is the most common method of determining the carrier density and mobility of semiconductor materials. Multicarrier characterization techniques are needed for determination of carrier densities and mobilities in a multicarrier system present in layered structures or in a variety of complex semiconductor materials. Because of the importance of these methods for proper electrical characterization of complex HgCdTe single crystals or layered structures, we discuss this topic pedagogically with the primary objective of promulgation of this emerging tool to the HgCdTe characterization community. We also discuss magnetoresistance and magnetoresistance-based techniques such as the Shubnikov-de Haas effect and magnetophonon effect, which have been used to characterize HgCdTe materials. These techniques are all capable of providing very accurate data if applied with care and proper analysis.
[Contact: Jeremiah R. Lowney, (301) 975-2048]

Nelson, A.J., Bode, M., Horner, G., Sinha, K., and Moreland, J., **Epitaxial Growth and Characterization of the Ordered Vacancy Compound $CuIn_3Se_5$ on GaAs (100) Fabricated by Molecular Beam Epitaxy**, Proceedings of the Materials Research Society Symposium, Vol. 340, pp. 599-603 (1994).

Epitaxial growth of the ordered vacancy compound (OVC) $CuIn_3Se_5$ has been achieved on GaAs (100) by molecular beam epitaxy from Cu_2Se and In_2Se_3 sources. Electron probe microanalysis and X-ray diffraction have confirmed the composition for the 1-3-5 OVC phase and that the film is single-crystal $CuIn_3Se_5$ (100). Transmission electron microscopy characterization of the material also showed it to be single crystalline. Structural defects in the layer consisted mainly of stacking faults. Photoluminescence measurements performed at 7.5 K indicate that the bandgap is 1.28 eV. Raman spectra reveal a strong polarized peak at 152 cm^{-1}, which is believed to arise from the totally symmetric vibration of the Se atoms in the lattice. Atomic force microscopy reveals faceting in a preferred (100) orientation.
[Contact: John Moreland, (303) 497-3641]

Analysis and Characterization Techniques

Released for Publication

Hopkins, P.F., Thomson, R.E., Moreland, J., Malhotra, S.S., and Liou, S.H., **Magnetic Force Microscopy Using Fe-(SiO_2) Coated Tips**, to be published in the Digest of the 1995 International Magnetics Conference, San Antonio, Texas, April 18-21, 1995.

[See Magnetic Materials and Measurements.]

Kim, J.S., Seiler, D.G., Colombo, L., and Chen, M.C., **Characterization of Liquid-Phase Epitaxially Grown HgCdTe Films by Magnetoresistance Measurements**.

In this paper, we demonstrate that measurements of the magnetoresistance can be used as a valuable alternative to conventional characterization tools to study transport properties of advanced semiconducting materials, structures, or devices. We have measured magnetoresistance on two different systems, namely, three liquid-phase epitaxially grown HgCdTe films and two GaAs-based high-electron-mobility-transistor (HEMT) structures. The results are analyzed by using a two-carrier model as a reference in the context of the reduced-conductivity-tensor scheme. The HEMT data are in quantitative agreement with the two-carrier model, but the HgCdTe data exhibit appreciable deviations from the model. The observed deviations strongly indicate a mobility spread and material complexity in the HgCdTe samples which are probably associated with inhomogeneities and the resulting anomalous behavior.
[Contact: Jin S. Kim, (301) 975-2238]

Rice, P., and Moreland, J., **Comparison of Magnetic Force Microscopy Techniques**, to be published in the Digest of the 1995 International Magnetics Conference, San Antonio, Texas, April 18-21, 1995.

[See Magnetic Materials and Measurements.]

Schaafsma, D.T., and Christensen, D.H., **Cross-Sectional Photoluminescence and Its Application to Buried-Layer Semiconductor Structures**.

We present an overview of a cross-sectional scanning microphotoluminescence technique. This technique is used to examine various buried-layer semiconductor structures for which traditional surface-normal techniques cannot yield sufficient information or must be coupled with time-consuming and painstaking processes such as wet etching. This technique has a wide range of applications; two, defect-driven interdiffusion in quantum wells and the modification of spontaneous emission from quantum wells in vertical-cavity surface-emitting lasers (VCSELs), are discussed here. The data obtained using this method can be used to distinguish emission spectra from quantum wells as little as 1 μm apart in depth and a few nanometers different in wavelength. The comparison of normal-incidence with cross-sectional data from VCSELs can be used to more effectively optimize the match between cavity resonance and quantum-well emission in high-Q devices. The physical model for an oscillating dipole in a planar cavity leads to an interesting conclusion about the dependence of the emission spectrum on the location of the dipole, namely, that an emitter inside a Fabry-Perot cavity will have the same spectrum as an identical one located a corresponding distance outside of the cavity. This conclusion is tested experimentally, using a VCSEL structure with emitters distributed inside and outside the effective cavity length.
[Contact: David H. Christensen, (303) 497-3354]

Thomson, R.E., and Moreland, J., **Development of High Conductive Cantilevers for Atomic Force Microscopy Point Contact Measurements**.

We have investigated several techniques for improving the electrical conductivity of micromachined silicon cantilevers for atomic force microscopy point contact measurements. The techniques studied included sputtering or evaporating thin layers of gold, platinum, or silver onto the lower surface of the cantilever to create a conducting metal layer, and doping the cantilevers with phosphorus. We have found that the lowest resistance contacts to a gold surface can be made by the metal-coated tips, which can make point contacts with resistances as low as 30 Ω at a tip-sample force of 15 μN.
[Contact: Ruth E. Thompson, (303) 497-3141]

Thomson, R.E., Moreland, J., and Roshko, A., **Five Distinct Methods for Surface Modification of YBCO Thin Films with the Scanning Tunneling Microscope**.

[See Cryoelectronic Metrology.]

Analysis and Characterization Techniques

Recently Published

Baker-Jarvis, J., and Janezic, M.D., **Open-Ended Coaxial Probes for Nondestructive Testing of Substrates and Circuit Boards**, Proceedings of the Materials Research Society Symposium, Vol. 347, pp. 215-220 (1994).

[See Electromagnetic Properties.]

Baker-Jarvis, J., Janezic, M.D., Domich, P.D., and Geyer, R.G., **Analysis of an Open-Ended Coaxial Probe with Lift-Off for Nondestructive Testing**, IEEE Transactions on Instrumentation and Measurement, Vol. 43, No. 5, pp. 711-718 (October 1994).

[See Electromagnetic Properties.]

Cavicchi, R.E., Suehle, J.S., Chaparala, P., Kreider, K.G., Gaitan, M., and Semancik, S., **Micro-Hotplate Gas Sensor**, Proceedings of the Solid-State Sensor and Actuator Workshop, Hilton Head, South Carolina, June 13-16, 1994, pp. 53-56.

Micro-hotplates have been fabricated on a silicon wafer using CMOS technology. These micromachined devices offer a wide range of temperature control, from 20 °C to 550 °C or 1000 °C, depending on design materials, and a fast thermal response of about 1 ms. They may be fabricated in arrays with electrical circuitry on the same chip. To make sensors from CMOS chips or wafers requires a new technology for processing, which include anisotropic etching of Si, lithography, and film deposition. All process steps must be compatible with existing CMOS components and structures and must take into account the geometry and stability of micromachined structures. For gas sensors that use semiconducting oxides, the challenge is to make ohmic contacts that use a very small contact area and are rugged against thermal cycling. The micro-hotplate array can serve as a mini-laboratory for efficient process optimization using parallel experiments. The elements of a micro-hotplate array can be programmed with different temperature schedules through the process steps, and subsequently analyzed in one test/characterization cycle. An example of a film growth study is shown in which array elements are set to different temperatures during sputter deposition of tin oxide. The rapid thermal time constant of these structures offers opportunities for new modes of sensor operation which can reduce the power consumption and improve the selectivity of oxide sensors. Techniques that use temperature pulses are demonstrated for low power sensing of H_2 in air and for distinguishing ethanol from methanol vapor.
[Contact: John S. Suehle, (301) 975-2247]

Cavicchi, R.E., Suehle, J.S., Chaparala, P., Poirier, G.E., Kreider, K.G., Gaitan, M., and Semancik, S., **Micro-Hotplate Temperature Control for Sensor Fabrication, Study, and Operation**, Proceedings of the Fifth International Meeting on Chemical Sensors, Rome, Italy, July 11-14, 1994, pp. 1136-1139.

Micro-hotplates have been fabricated on a silicon wafer using CMOS technology. These micromachined devices offer a wide range of temperature control, from 20 °C to 550 °C or 1000 °C, depending on design materials, and a fast thermal response of about 1 ms. They may be fabricated in arrays with electrical circuitry on the same chip. Micro-hotplates are useful both as platforms for scientific studies related to chemical sensors and as building blocks for array sensors. We present results using micro-hotplates to study sensor film growth and reaction kinetics. We also demonstrate the potential for temperature-pulsed-sensing modes which can reduce power consumption.
[Contact: John S. Suehle, (301) 975-2247]

Christensen, D.H., Hickernell, R.K., Schaafsma, D.T., Pellegrino, J.G., McCollum, M.J., Hill, J.R., and Rai, R.S., **Correlation of Optical, X-Ray, and Electron Microscopy Measurements on Semiconductor Multilayer Structures**, Proceedings of SPIE (The International Society for Optical Engineering, P.O. Box 10, Belllingham, Washington 98227-0010), Optical Engineering/Laser Application and Science Engineering, Vol. 2141, pp. 177-188 (1994).

Techniques based on optical, X-ray, and electron

microscopy measurements are applied to characterize a wide variety of semiconductor multilayer structures. Bragg mirrors serve as valuable test structures for evaluating the epitaxial uniformity of crystal growth systems. Careful characterization of half-wave spaced single quantum wells provides a method for determining their complex refractive indices using reflectance spectroscopy. Comparison of cross-sectional microphotoluminescence to surface-normal photoluminescence, combined with these characterization techniques, allows studies of spontaneous emission in microcavities and elucidates the difficulties with using surface-normal photoluminescence to determine the alloy composition of the mirror layers. The application of these characterization methods to visible-wavelength AlGaAs mirrors, 485 to 720 nm, enables the development of these mirrors for uses such as optically tailored substrates and visible surface-emitter of detector arrays.
[Contact: David H. Christensen, (303) 497-3354]

Diebold, A.C., Kump, M., Kopanski, J.J., and Seiler, D.G., **Characterization of Two-Dimensional Dopant Profiles: Status and Review**, Proceedings of the Electrochemical Society, Miami, Florida, October 10-14, 1994, pp. 78-97.

[See Device Physics and Modeling.]

Kopanski, J.J., Marchiando, J.F., Lowney, J.R., and Seiler, D.G., **Scanning Capacitance Microscopy for Profiling PN-Junctions in Silicon**, Workshop Summary Report: Industrial Applications of Scanned Probe Microscopy, J. A. Dagata, A. C. Diebold, C. K. Shih, and R. J. Colton, Eds., NISTIR 5550, pp. 63-64 (December 1994).

The NIST scanning capacitance microscope combines an atomic force microscope (AFM) with a high-sensitivity capacitance measurement. A metallized AFM tip, separated by an air gap and oxide layer from a semiconductor, is used to form a metal-insulator-semiconductor capacitor. As the cantilever tip of the AFM is scanned over a semiconductor surface, topography and capacitance are measured simultaneously, permitting capacitance measurements limited in spatial resolution by the tip radius. The RCA videodisc sensor is used for capacitance detection.
[Contact: Joseph J. Kopanski, (301) 975-2089]

Perkowitz, S., Seiler, D.G., and Duncan, W.M., **Optical Characterization In Microelectronics Manufacturing**, J. Res. Inst. Stand. Technol., Vol. 99, No. 5, pp. 605-639 (September-October 1994).

To successfully construct semiconductor devices, the semiconductor industry must measure fundamental material parameters, especially when developing new materials; measure the quality of the material as it is grown; accurately determine the details of thin films, quantum wells, and other microstructures that control or affect device performance; and measure properties of the devices themselves. Properties that need to be determined, therefore, include basic band structure and transport parameters, such as energy gap values and carrier scattering times; the presence and concentration of impurities and defects; alloy parameters; layer thickness; the distribution of materials in complex structures; and many others. This process of determining a wide range of material, structural, and device parameters is called characterization. The semiconductor industry uses many characterization methods which draw on electrical, chemical, and other approaches. Among these, optical characterization techniques, defined as those using electromagnetic radiation from the ultraviolet to the far infrared, stand out because they are nondestructive and require minimal sample preparation since no contacts are needed. These features are of great importance for production use or to examine finished devices. Another benefit is that, unlike electrical methods which require fixed contacts, optical techniques can give two- or three-dimensional maps of properties over the extent of a semiconductor wafer. The six techniques described in this paper (ellipsometry, infrared spectroscopy, microscopy, modulation spectroscopy, photoluminescence, and Raman scattering) were chosen because they are currently or potentially widely used in the industry; they measure a broad array of semiconductor parameters; and they operate in different regions of the electromagnetic spectrum. The discussion of each technique indicates the basic semiconductor quantities measured, gives the scientific basis of the technique, and indicates how the measurement is made. Illustrative examples from the literature are discussed in detail, showing applications to important semiconductor materials. More information can be obtained from the detailed list of references included. References listed under

"General" give a broad overview of the technique, its theory, and practice. Those under "Applications" present further illustrations of how the technique is used for specific problems in real materials, primarily Si, GaAs, AlGaAs, but also diamond, SiO_2, GaAs/Si, InSb, GaAsSb, InGaAs, InGaAlAs, CdTe, HgCdTe, AlAs/GaAs, and HgTe/CdTe.
[Contact: David G. Seiler, (301) 975-6766]

Rice, P., and Moreland, J., **Flexible-Diaphragm Force Microscope**, Journal of Vacuum Science and Technology B, Vol. 12, No. 4, pp. 2465-2466 (July/August 1994).

[See Magnetic Materials and Measurements.]

Silver, R.M., Dagata, J.A., and Tseng, W.F., **Air and Ambient STM/S of Bulk-Doped GaAs and pn Junctions,** Workshop Summary Report: Industrial Applications of Scanned Probe Microscopy, J. A. Dagata, A. C. Diebold, C. K. Shih, and R. J. Colton, Eds., NISTIR 5550, pp. 99-100 (December 1994).

Characterization of local electronic properties and topography of semiconductor device structures is of increasing importance as critical dimensions are scaled down. Techniques must be developed to allow improved measurements of doping homogeneity, surface-state energy distributions and defect densities. The new class of scanned probe instruments, the scanning tunneling microscope (STM) in particular, makes possible nondestructive electronic measurements on the subnanometer scale with unparalleled resolution. Mapping the density of states of an individual defect, three-dimensional images of isolated dopants, and atomically resolved interfaces are only a few of the advances. Although these examples show the potential of the STM, it remains a challenge to make accurate, quantitative electrical measurements on real surfaces encountered in device fabrication since these surfaces have a substantial number of surface states or lack of atomic order.
[Contact: Wen F. Tseng, (301) 975-5291]

Yang, S., Vayshenker, I., Li, X., and Scott, T.R., **Accurate Measurement of Optical Detector Nonlinearity**, Proceedings of the National Conference of Standards Laboratories, Chicago, Illinois, July 31—August 4, 1994, pp. 353-362.

[See Photodetectors.]

Device Physics and Modeling

Released for Publication

Lowney, J.R., **Model for Determining the Density and Mobility of Carriers in Thin Semiconducting Layers with Only Two Contacts**.

A new method for determining the carrier densities and mobilities in a thin semiconducting layer is described. It is based on fitting the transverse magnetoresistance of the layers as a function of magnetic field, and it requires only two contacts. A computer code was written to solve for the magnetoresistance as a function of magnetic field and the length-to-width ratio of a rectangular sample. A nonlinear-least-squares fit was made to the results of the computer model for a single-carrier system. The results for multi-carrier systems are discussed. This method is especially useful as a monitor for improving the quality control of the electrical characteristics of thin conducting layers in finished devices.
[Contact: Jeremiah R. Lowney, (301) 975-2048]

Marchiando, J.F., **On Using Collocation in Three Dimensions and Solving a Model Semiconductor Problem**.

A research code has been written to solve an elliptic system of coupled nonlinear partial differential equations of conservation form on a rectangularly shaped three-dimensional domain. The code uses the method of collocation of Gauss points with tricubic Hermite piecewise continuous polynomial basis functions. The system of equations is solved by iteration. The system of nonlinear equations is linearized, and the system of linear equations is solved by iterative methods. When the matrix of the collocation equations is duly modified by using a scaled block-limited partial pivoting procedure of Gauss elimination, it is found that the rate of convergence of the iterative method is significantly improved and that a solution becomes possible. The code is used to solve Poisson's equation for a model semiconductor problem. The electric potential distribution is calculated in a metal-oxide-semiconductor structure that is important to the fabrication of electron devices.

[Contact: Jay F. Marchiando, (301) 975-2088]

Device Physics and Modeling

Recently Published

Dahmani, R., Salamanca-Riba, L.; Beesabathina, P., Nguyen, N.V., Chandler-Horowitz, D., and Jonker, B.T., **Characterization of the ZnSe/GaAs Interface Layer by TEM and Spectroscopic Ellipsometry**, Proceedings of the Materials Research Society Symposium, Vol. 280, pp. 271-274 (1993).

[See Insulators and Interfaces.]

Diebold, A.C., Kump, M., Kopanski, J.J., and Seiler, D.G., **Characterization of Two-Dimensional Dopant Profiles: Status and Review**, Proceedings of the Electrochemical Society, Miami, Florida, October 10-14, 1994, pp. 78-97.

Process and device simulators are being used for the technology computer-aided design (TCAD) of 0.25-μm gate-length transistors predicted to begin manufacture in 1998. This paper compares and reviews the status of inverse modeling and direct physical analysis methods to obtain two-dimensional dopant profiles for verification and calibration of these TCAD simulators. Spatial resolution, dopant accuracy, and concentration range requirements are discussed. Direct characterization methods include scanning probe microscopies (scanning capacitance microscopy, scanning tunneling microscopy combined with "spectroscopy," μ-spreading resistance probe, scanning Kelvin probe microscopy, and scanning potential microscopy), electron holography, tomographic secondary ion mass tomographic spectroscopy, spreading resistance profiling, and transmission electron microscopy of etched cross sections.
[Contact: Joseph J. Kopanski, (301) 975-2089]

Hefner, A.R., Jr., **A Dynamic Electro-Thermal Model for the IGBT**, IEEE Transactions on Industry Applications, Vol. 30, No. 2, pp. 394-405 (March/April 1994). [Also published in the Proceedings of the IEEE Industry Applications Society Annual Meeting, Houston, Texas, October 4-9, 1992, pp. 1094-1104.]

[See Power Devices.]

Hefner, A.R., Jr., **An Experimentally Verified IGBT Model Implemented in the Saber Circuit Simulator**, IEEE Transactions on Power Electronics, Vol. 9, No. 5, pp. 532-542 (September 1994). [Also published in the Proceedings of the 22nd Annual IEEE Power Electronics Specialists Conference, (PESC '91), Cambridge, Massachusetts, June 24-27, 1991, pp. 10-19.]

[See Power Devices.]

Hefner, A.R., and Blackburn, D.L., **Thermal Component Models for Electrothermal Network Simulation**, IEEE Transactions on Components, Packaging, and Manufacturing Technology, Part A, Vol. 17, No. 3 (September 1994). [Also published in the Proceedings of the Semiconductor Thermal Measurement and Management Symposium, Austin, Texas, February 2-4, 1993, pp. 88-96.]

A procedure is given for developing thermal component models for electro-thermal network simulation. In the new electrothermal network simulation methodology, the simulator solves for the temperature distribution within the semiconductor devices, packages, and heat sinks (thermal network) as well as the currents and voltages within the electrical network. The thermal network is represented as an interconnection of compact thermal component models so that the system designer can readily interchange different thermal components and examine different configurations of the thermal network. To facilitate electrothermal network design, the interconnection of the thermal component models is specified by the user in the same way that the interconnection of the electrical network components is specified. The thermal component models are also parameterized in terms of structural and material parameters so that the details of the heat transport physics are transparent to the user. Examples electrothermal network simulations are given, and the temperature measurement methods used to validate the thermal component models are described.
[Contact: Allen R. Hefner, (301) 975-2071]

Insulators and Interfaces

Recently Published

Chandler-Horowitz, D., Pellegrino, J.G., Nguyen, N.V., Amirtharaj, P.M., and Qadri, S.B., **Interface Roughness Induced Changes in the Near-E_o Spectroscopic Behavior of Short-Period GaAs/AlAs Superlattices**, Proceedings of the Materials Research Society Symposium, Vol. 326, pp. 145-149 (1994).

The perturbations on the optical properties introduced by increased interface roughness in 3 x 3 short-period AlAs/GaAs superlattices (SL) were investigated through an examination of the position and line shape of the E_o (direct gap) feature in photoreflectance (PR) and spectroscopic ellipsometry (SE). The degree of interface roughness in the SLs was controlled by a choice of the growth conditions and the buffer layer thickness. The structural behavior was characterized by X-ray diffraction. The measured spectra from PR and SE were compared to those from an $Al_xGa_{1-x}As$ ($x \approx 0.5$) alloy reference specimen grown under nearly identical conditions. The Γ and E_o values from the $Al_{0.5}Ga_{0.5}As$ alloy sample are valuable in this comparative analysis since they represent the lowest and highest bounds for the SL Γ and E_o, respectively. The results show that increasing interface roughness enlarges the linewidth, Γ from 42 meV to 64 meV, and the corresponding transition energy, E_o, shifts from 2,060 eV to 2.112 eV; the reference values from the SLs with increasing interface roughness may be understood as a consequence of the roughening-induced intermixing and the eventual reduction in the modulation depth of the SL potential. The increase of Γ also with roughening suggests the additional mechanisms, such as roughening-induced scattering, are important.
[Contact: Deane Chandler-Horowitz, (301) 975-2084]

Dahmani, R., Salamanca-Riba, L.; Beesabathina, P., Nguyen, N.V., Chandler-Horowitz, D., and Jonker, B.T., **Characterization of the ZnSe/GaAs Interface Layer by TEM and Spectroscopic Ellipsometry**, Proceedings of the Materials Research Society Symposium, Vol. 280, pp. 271-274 (1993).

The interface between ZnSe thin films and GaAs substrates is characterized by high-resolution transmission electron microscopy and room-temperature spectroscopic ellipsometry. The films were grown on (001) GaAs by molecular beam epitaxy. A three-phase model is used in the reduction of the ellipsometric data from which the presence of a transition layer of Ga_2Se_3, with a thickness of less than 1 nm, is confirmed. These results corroborate the high-resolution transverse electromagnetic microscopy images obtained from the same samples.
[Contact: Nahn Van Nguyen, (301) 975-2044]

Witczak, S.C., Gaitan, M., Suehle, J.S., Peckerar, M.C., and Ma, D.I., **The Interaction of Stoichiometry, Mechanical Stress, and Interface Trap Density In LPCVD Si-Rich SiN_x-Si Structures**, Solid-State Electronics, Vol. 37, No. 10, pp. 1695-1704 (1994).

Mechanical and electrical properties were correlated in LPCVD SiN_x-Si structures through the characterization of six wafers patterned with MNS capacitors whose insulator films were deposited rich in Si under various processing conditions. The samples were measured for mechanical stress at the Si-SiN_x interface with X-ray diffraction. The deposited SiN_x films were measured for stoichiometry by Rutherford backscattering spectroscopy. Low-temperature C-V measurements were used for the first time to estimate Si-SiN_x interface trap densities in the capacitors. The interface trap densities were confirmed with the aid of a model based on a numerical analysis of the capacitor small-signal response. The measurement results indicate that an increase in the Si/N ratio in the insulating films was accompanied by a decrease in the film tensile stress. Those SiN_x films made sufficiently rich in Si were successfully deposited under compressive stress. Furthermore, a decrease in the magnitude of the stress was accompanied by a decrease in interface trap densities, suggesting that interfacial mechanical stress may be influential in the formation of Si-SiN_x interface traps. Interface trap densities were lowest in those structures whose insulating films were deposited under compression.
[Contact: Michael Gaitan, (301) 975-2070]

Dimensional Metrology

Released for Publication

Brilliant, N.A., and Young, M., **Video Microscopy**

Applied to Optical Fiber Geometry Measurements, NIST Technical Note 1369 (November 1994).

[See Optical Fiber Metrology.]

Dimensional Metrology

Recently Published

Drapela, T.J., Franzen, D.L., and Young, M., **Fiber Geometry: Results of an International Interlaboratory Measurement Comparison**, in Technical Digest - Symposium on Optical Fiber Measurements, 1994, NIST Special Publication 864, G. W. Day, D. L. Franzen, and R. K. Hickernell, Eds. (September 1994), pp. 129-132.

[See Optical Fiber Metrology.]

Postek, M.T., Lowney, J.R., Vladar, A.E., Keery, W.J., Marx, E., and Larrabee, R.D., **Electron Beam Interaction Modeling as Applied to X-Ray Lithography Mask SEM Linewidth Metrology**, Scanning, Vol. 16, Supp. IV, pp. IV-56-IV-57 (1994).

Accurate dimensional metrology of the submicrometer gold absorber structures of X-ray masks can be accomplished in the scanning electron microscope (SEM) with the use of electron beam modeling. Accurate metrology is possible because the X-ray masks present a unique measurement object from most other semiconductor structures viewed in the SEM. This occurs because the silicon support membrane is X-ray transparent by design. This characteristic can be used as a distinct advantage in electron beam-based mask metrology since, depending upon the incident electron beam energies, substrate composition, and substrate thickness, the membrane can also be essentially electron-transparent. The areas of the mask where the absorber structures are located are essentially X-ray-opaque, as well as electron-opaque. Viewing the sample from a perspective below the mask by placing an electron detector beneath the mask provides excellent electron signal contrast between the absorber structure and the base membrane. The present technique utilizes a broad acceptance angle detector which is different in concept from other transmission electron detectors used in the SEM.
[Contact: Jeremiah R. Lowney, (301) 975-2048]

Wang, C.M., Vecchia, D.F., Young, M., and Brilliant, N.A., **Software for Performing Gray-Scale Measurements of Optical Fiber End Faces**, NIST Technical Note 1370 (November 1994).

[See Optical Fiber Metrology.]

Integrated-Circuit Test Structures

Released for Publication

Schafft, H.S., Mayo, S., Jones, S.N., and Suehle, J.S., **An Electrical Method for Determining the Thickness of Metal Films and the Cross-Sectional Area of Metal Lines**, to be published in the Proceedings of the 1994 Integrated Reliability Workshop, Lake Tahoe, California, October 16-19, 1994.

[See Reliability.]

Integrated-Circuit Test Structures

Recently Published

Linholm, L.W., Allen, R.A., and Cresswell, M.C., **Microelectronic Test Structures for Feature Placement and Electrical Linewidth Metrology**, in Critical Reviews of Optical Science and Technology, Handbook of Critical Dimension Metrology and Process Control, Vol. CR52, K. M. Monahan, Ed. (SPIE, Bellingham, Washington, 1994), pp. 91-118.

This paper presents a critical review of electrical test methods for determining feature placement with total measurement uncertainties below 10 nm and electrical linewidth for sub-half-micrometer design linewidths with measurement precision below 1 nm. Control of feature placement and control of linewidth have been and are expected to continue to be two of the most important challenges required in the manufacturing of advanced microelectronic devices. Traditional methods of measuring these parameters suffer from both measurement speed and equipment expense. Microelectronic test structures are electrical devices that are used to determine selected tool, process, device, material, or circuit

parameters by means of electrical tests. They are supported by a variety of commercial test equipment often found in semiconductor manufacturing facilities. They provide low-cost, post-patterning metrology for determining both feature placement and electrical linewidth. Properly characterized test structures and measurement methods provide an economic means of determining the critical parameters needed to develop, control, and operate the next generation of patterning tools.
[Contact: Loren W. Linholm, (301) 975-2052]

Microfabrication Technology

Released for Publication

Cavicchi, R.E., Suehle, J.S., Kreider, K.G., Chaparala, P., and Gaitan; M., **Fast Temperature Programmed Sensing for Micro-Hotplate Gas Sensors**.

We describe an operating mode of a gas sensor that greatly enhances the capability of the device to determine the composition of a sensed gas and can enhance the sensitivity of the device to lower concentrations of a test gas. The device consists of a micromachined hotplate with integrated heater, heat distribution plate, electrical contact pads, and sensing film. The temperature-programmed-sensing technique uses millisecond time-scale temperature changes to control the kinetics for adsorption, desorption, and reaction of gases on the surface. To overcome the problem of a simple temperature-dependent conductance based on the thermal activation of carriers, device conductance is measured at a fixed temperature. Temperature pulses are applied between conductance measurements. A repetitive pulse train produces a patterned conductance response that depends on the gas composition, as well as the temperature pulse width, amplitude, and specific sequence of pulses. Temperature pulses are also used to enhance a sensor response. Results are shown for ethanol, methanol, formaldehyde, acetone, and CO.
[Contact: John S. Suehle, (301) 975-2247]

Sauvageau, J.E., Booi, P.A.A., Cromar, M.W., Benz, S.P., Burroughs, C.J., and Koch, J.A., **Superconducting Integrated Circuit Fabrication Process Utilizing Low-Temperature ECR-Based PECVD SiO_2 Dielectric Films**, to be published IEEE Transactions on Applied Superconductivity, Proceedings of the Applied Superconductivity Conference, Boston, Massachusetts, October 16-21, 1994.

A superconducting integrated circuit fabrication process has been developed to encompass a wide range of applications such as Josephson voltage standards, VLSI scale array oscillators, SQUIDs, and kinetic inductance based devices. An optimal Josephson junction process requires low-temperature processing for all deposition and etching steps. This low-temperature process involves an electron-cyclotron-resonance-(ECR-)-based plasma-enhanced chemical vapor deposition (PECVD) of SiO_2 films for interlayer dielectrics. Experimental design and statistical process control techniques have been used to ensure high-quality oxide films. Oxide and niobium etch processes include endpoint detection and controlled overetch of all films. An overview of the fabrication process is presented.
[Contact: Joseph E. Sauvageau, (303) 497-3770]

Microfabrication Technology

Recently Published

Cavicchi, R.E., Suehle, J.S., Chaparala, P., Kreider, K.G., Gaitan, M., and Semancik, S., **Micro-Hotplate Gas Sensor**, Proceedings of the Solid-State Sensor and Actuator Workshop, Hilton Head, South Carolina, June 13-16, 1994, pp. 53-56.

[See Analysis and Characterization Techniques.]

Cavicchi, R.E., Suehle, J.S., Chaparala, P., Poirier, G.E., Kreider, K.G., Gaitan, M., and Semancik, S., **Micro-Hotplate Temperature Control for Sensor Fabrication, Study, and Operation**, Proceedings of the Fifth International Meeting on Chemical Sensors, Rome, Italy, July 11-14, 1994, pp. 1136-1139.

[See Analysis and Characterization Techniques.]

Thomson, R.E., Moreland, J., and Roshko, A., **Surface Modification of $YBa_2Cu_3O_{7-\delta}$ Thin Films Using the Scanning Tunneling Microscope: Five Methods**, Nanotechnology, Vol. 5, pp. 57-69 (1994).

[See Cryoelectronic Metrology.]

Plasma Processing

Released for Publication

Radovanov, S.B., Olthoff, J.K., Van Brunt, R.J., and Djurovic, S., **Ion Kinetic-Energy Distributions and Balmer-Alpha (H_α) Excitation in Ar-H_2-Radio-Frequency Discharges**.

Excited neutrals and fast ions produced in a 13.56-MHz radio-frequency discharge in a 90% argon - 10% hydrogen gas mixture were investigated, respectively, by spatially and temporally resolved optical emission spectroscopy, and mass-resolved measurement of ion kinetic energy distributions at the grounded electrode. The electrical characteristics of the discharge were also measured, and comparisons are made with results obtained for discharges in pure H_2 under comparable conditions. Measurements of Balmer-alpha (H_α) emission show Doppler shifted emission that is due to the excitation of fast atomic hydrogen neutrals formed from ion neutralization processes in the discharge. Temporally and spatially resolved emission profiles of the H_α radiation are presented for the "slow" component produced predominately by electron-impact dissociative excitation of H_2, and for the "fast" component corresponding to energies much greater than can be derived from dissociative excitation. When argon is added to hydrogen, the fast component is significantly enhanced relative to the slow component. The measured kinetic-energy distributions and fluxes of predominantly ions in the Ar-H_2 mixture, such as H_3^+, H_2^+, H^+, and ArH^+, suggest mechanisms for the formation of fast hydrogen atoms. The interpretation of results indicate that H^+ and/or H_3^+, neutralized and backscattered by collision with the powered electrode, are the likely sources of fast hydrogen atoms that produce Doppler-shifted H_α emission in the discharge. There is also evidence at the highest pressures and voltages of "runaway" H^+ ions formed near the powered electrode, and detected with kinetics energies exceeding 100 eV at the grounded electrode.
[Contact: James K. Olthoff, (301) 975-2431]

Power Devices

Recently Published

Blackburn, D.L., **Status and Trends in Power Semiconductor Devices**, Proceedings of the IEEE International Conference on Industrial Electronics (IECON '93), Lahaina, Maui, Hawaii, November 15-19, 1993, pp. 619-625 (1994).

A brief description of some recent developments that affect the application of power semiconductor devices is given. Developments in chips, packages, simulation, and new materials are included.
[Contact: David L. Blackburn, (301) 975-2053]

Hefner, A.R., Jr., **A Dynamic Electro-Thermal Model for the IGBT**, IEEE Transactions on Industry Applications, Vol. 30, No. 2, pp. 394-405 (March/April 1994). [Also published in the Proceedings of the IEEE Industry Applications Society Annual Meeting, Houston, Texas, October 4-9, 1992, pp. 1094-1104.]

A physics-based dynamic electro-thermal model is developed for the IGBT by coupling a temperature-dependent IGBT electrical model with dynamic thermal models for the IGBT silicon chip, packages, and heatsinks. The temperature-dependent IGBT electrical model describes the instantaneous electrical behavior in terms of the instantaneous temperature of the IGBT silicon chip surface. The instantaneous power dissipated in the IGBT is calculated using the electrical model and determines the instantaneous rate that heat is applied to the surface of the silicon chip thermal model. The thermal models determine the evolution of the temperature distribution within the thermal network, and thus determine the instantaneous value of the silicon chip surface temperature used by the electrical model. The IGBT electro-thermal model is implemented in the Saber circuit simulator and is connected to external circuits in the same way as the previously presented Saber IGBT model, except that it has an additional thermal terminal that is connected to the thermal network component models for the silicon chip, package, and heatsink. The IGBT dynamic electro-thermal model and the thermal network component models are verified for the range of temperature and power dissipation levels (heating rates) that are important for power electronic systems.
[Contact: Allen R. Hefner, Jr., (301) 975-2071]

Hefner, A.R., Jr., **An Experimentally Verified IGBT Model Implemented in the Saber Circuit Simulator**, IEEE Transactions on Power Electronics, Vol. 9, No. 5, pp. 532-542 (September 1994). [Also published in the Proceedings of the 22nd Annual IEEE Power Electronics Specialists Conference, (PESC '91), Cambridge, Massachusetts, June 24-27, 1991, pp. 10-19.]

A physics-based IGBT model is implemented into the general purpose circuit simulator Saber. The IGBT model includes all of the physical effects that have been shown to be important for describing IGBTs, and the model is valid for general external circuit conditions. The Saber IGBT model is evaluated for the range of static and dynamic conditions in which the device is intended to be operated, and the simulations compare well with experimental results for all of the conditions studied. [Contact: Allen R. Hefner, Jr., (301) 975-2077]

Hefner, A.R., and Blackburn, D.L., **Thermal Component Models for Electrothermal Network Simulation**, IEEE Transactions on Components, Packaging, and Manufacturing Technology, Part A, Vol. 17, No. 3 (September 1994). [Also published in the Proceedings of the Semiconductor Thermal Measurement and Management Symposium, Austin, Texas, February 2-4, 1993, pp. 88-96.]

[See Device Physics and Modeling.]

Photodetectors

Released for Publication

Lowney, J.R., **Model for Determining the Density and Mobility of Carriers in Thin Semiconducting Layers with Only Two Contacts**.

[See Device Physics and Modeling.]

Photodetectors

Recently Published

Kim, J.S., Seiler, D.G., Colombo, L., and Chen, M.C., **Electrical Characterization of Liquid-Phase Epitaxially Grown Single-Crystal Films of Mercury Cadmium Telluride by Variable Magnetic-Field Hall Measurements**, Semiconductor Science and Technology, Vol. 9, pp. 1696-1705 (1994).

[See Compound Materials.]

Lowney, J.R., Kim, J.S., and Seiler, D.G., **Magnetotransport Properties of HgCdTe**, EMIS Data Review, in Properties of Narrow Gap Cadmium-Based Compounds, Chapter A6.12, P. Capper, Ed. (INSPEC, London, 1994), pp. 264-270.

[See Compound Materials.]

Rice, J.P., Grossman, E.N., and Rudman, D.A., **Antenna-Coupled High-T_c Air-Bridge Microbolometer on Silicon**, Applied Physics Letters, Vol. 65, No. 6, pp. 773-775 (August 1994).

[See Cryoelectronic Metrology.]

Yang, S., Vayshenker, I., Li, X., and Scott, T.R., **Accurate Measurement of Optical Detector Nonlinearity**, Proceedings of the National Conference of Standards Laboratories, Chicago, Illinois, July 31—August 4, 1994, pp. 353-362.

In this paper, we describe the results of our efforts to analyze and compare by computer simulation three popular nonlinearity methods: (1) superposition method, (2) attenuation method, and (3) differential or ac-dc method. We describe a uniform definition which we used to intercompare the data analysis properties of these methods. Issues, common to these methods or specific to one individual method, that have an impact on the measurement accuracy were studied. We conclude that superposition and differential methods are better choices than the attenuation method. Suggestions about the choice of polynomial order of the fitting curve with regard to the data accuracy and detector nonlinearity are also given.
[Contact: Thomas R. Scott, (303) 497-3651]

Reliability

Released for Publication

Schafft, H.S., Mayo, S., Jones, S.N., and Suehle, J.S., **An Electrical Method for Determining the Thickness of Metal Films and the Cross-Sectional Area of Metal Lines**, to be published in

the Proceedings of the 1994 Integrated Reliability Workshop, Lake Tahoe, California, October 16-19, 1994.

The electrical thickness of an aluminum-alloy metallization can be determined from resistance measurements of a van der Pauw cross structure at two temperatures, with corrections for the deviation from Matthiessen's rule and for thermal expansion. Thickness determinations made in this way agree with those made with a calibrated SEM to within the uncertainty of the instrument. The electrical cross-sectional area of metal lines can be determined by making resistance measurements at two temperatures.
[Contact: Harry S. Schafft, (301) 975-2234]

Other Semiconductor Metrology Topics

Recently Published

Amirtharaj, P.M., and Seiler, D.G., **Optical Properties of Semiconductors**, in Handbook of Optics, Vol. II, Devices, Measurements, and Properties, Second Edition, Chapter 36, M. Bass, E. W. Van Stryland, D. R. Williams, and W. L. Wolfe, Eds. (McGraw-Hill, New York, 1994), pp. 36.1-36.96.

All optical measurements of semiconductors rely on a fundamental understanding of their optical properties. A broad overview of the optical properties is given, along with numerous specific examples.
[Contact: Paul M. Amirtharaj, (301) 975-5974]

Scace, R.I., **Measurements - What Next?** Solid-State Technology, pp. 43-47 (March 1994).

Semiconductor manufacturing is evolving from being an empirical art into an industry based increasingly on physical understanding and real-time process control. Both understanding and control require correctly applied measurement tools, many of which do not now exist in suitable form. In addition, the continuing drive toward smaller geometries and more complex chips leads directly to demands on metrology that cannot be met using refinements of today's technology. New approaches to measurement will often be necessary.
[Contact: Robert I. Scace, (301) 975-4400]

SIGNAL ACQUISITION, PROCESSING, AND TRANSMISSION

DC and Low-Frequency Metrology

Released for Publication

Clark, A.F., and Steiner, R.L., **Noise Characteristics Below 1 Hz of Zener Diode-Based Voltage References**, to be published an Abstract in the Bulletin of the American Physical Society Meeting, San Jose, California, March 13-17, 1995.

The short- and mid-term noise of voltage references based on Zener diodes are the limiting factors in the accuracy of their application as voltage standards. Although these references are relatively rugged, survive the rigors of shipping, and have predictable long-term behavior, they do have noise in the voltage output values with a time dependence about the same as the desired measurement intervals. We have characterized several of these references in the frequency range of 10^{-1} to 10^{-6} Hz (time intervals of seconds to months) by direct comparison to a Josephson array voltage standard at the 10- and 1-V level with nanovolt precision. Several distinctly different regions of noise characteristics are observed. Comparisons are made with 1/f and other expected behaviors and resulting accuracy limitations are discussed.
[Contact: Alan F. Clark, (301) 975-2139]

Oldham, N.M., **Overview of Bioelectrical Impedance Analyzers**, to be published in the Proceedings of the Technology Assessment Conference on Bioelectrical Impedance Analysis in Body Composition Measurement, Bethesda, Maryland, December 12, 1994.

Bioelectrical impedance analyzers (BIAs) are used to measure human body impedances to predict the ratio of body water and body fat relative to height and weight. Five BIAs were evaluated to determine the accuracy of these instruments as electrical impedance meters. Preliminary tests indicate that at impedances around 500 Ω (typical human body impedance at 50 kHz) BIA, uncertainties range from 2% to 15%.
[Contact: Nile M. Oldham, (301) 975-2408]

DC and Low-Frequency Metrology

Recently Published

Lee, K.C., Cage, M.E., and Rowe, P.S., **Sources of Uncertainty in a DVM-Based Measurement System for a Quantized Hall Resistance Standard**, J. Res. Natl. Inst. Stand. Technol., Vol. 99, No. 3, pp. 227-240 (May—June 1994).

Transportable 10-kΩ standard resistors have become fairly widespread in industrial, university, and government standards laboratories because of their low-temperature coefficient of resistance, ease of transportation, and convenient value. The values of these resistors, however, tend to drift with time, requiring periodic recalibration against an absolute standard such as the quantized Hall resistance. The availability of a simple, inexpensive measurement system for calibrating 10-kΩ resistors against this absolute standard would be of great benefit to such primary standards laboratories. This paper describes a simple automated measurement system using a single, high-accuracy, commercially available digital voltmeter to compare the voltages developed across a 10-kΩ standard resistor and a quantized Hall resistor when the same current is passed through the two devices. From these measurements, the value of the 10-kΩ standard resistor is determined. The sources of uncertainty in this system are analyzed in detail, and it is shown that it is possible to perform calibrations with uncertainties in the range of 0.1 ppm.
[Contact: Kevin C. Lee, (301) 975-4236]

Waveform Metrology

Released for Publication

Paulter, N.G., **An Electrooptic-Based RMS Voltage Measurement Technique**.

A new electrooptic-based technique for measuring the rms value of an applied voltage is presented. The technique incorporates a ratiometric method whereby the requirement for absolute laser power information is unnecessary. A description, analysis, and experimental results of the prototype measurement system are presented.
[Contact: Nicholas G. Paulter, Jr., (301) 975-2405]

Cryoelectronic Metrology

Released for Publication

Berkowitz, S.J., Antognazza, L., Char, K., Ono, R.H., Missert, N., Rosenthal, P.A., Vale, L.R., Mankiewich, P.M., and Skocpol, W.J., **Interface Scattering in High-Temperature Superconducting-Normal-Superconducting Josephson Junctions**.

We have fabricated $YBa_2Cu_3O_{7-\delta}$-normal metal $YBa_2Cu_3O_{7-\delta}$ step-edge and edge-Josephson junctions that fit an SINIS model. Both the low- and high-bias behavior is consistent with a mixed transparency interface that can be modeled as a semi-transparent insulator. We demonstrate that an interface dominated SNS junction is expected to have a higher critical current-normal resistance (I_cR_N) product at 77 K than a proximity coupled one.
[Contact: Ronald H. Ono, (303) 497-3762]

Benz, S.P., Reintsema, C.D., Ono, R.H., Eckstein, J.N., Bozovic, I., and Virship, G.F., **Step-Edge and Stacked-Heterostructure High-T_c Josephson Junctions for Voltage Standard Arrays**.

We have explored two high-transition-temperature Josephson junction technologies for application in voltage standard arrays: the step-edge junctions made with $YBa_2Cu_3O_{7-\delta}$ and Au normal-metal bridges and stacked series arrays of Josephson junctions in selectively doped, epitaxially grown $Bi_2Sr_2CaCu_2O_8$ heterostructures. For both kinds of junctions, Shapiro steps induced by a microwave bias were characterized as a function of power. We compare the two technologies with respect to critical current and normal resistance uniformity, maximum achievable critical current, critical-current normal-resistance product, and operation temperature.
[Contact: Samuel P. Benz, (303) 497-5258]

Booi, P.A.A., and Benz, S.P., **Resonances in Two-Dimensional Array Oscillator Circuits**.

We present experimental results on the emission from phase-locked two-dimensional arrays of Josephson junctions. We have coupled the emission from 10 x 10 arrays to a room-temperature mixer through a fin-line antenna and WR-12 waveguide. A single voltage-tunable peak was detected up to 230 GHz. A stripline resonance in

the antenna reduced the array's dynamic resistance, and thereby the emission linewidth, to as low as 10 kHz. We extract an effective noise temperature of 14 K from the linewidth data. When the array's emission was coupled to an on-chip detector junction through a dc blocking capacitor, we detected voltage-tunable emission from 75 GHz up to 300 GHz, and in some circuits emission above 400 GHz. The coherent power spectrum depends primarily on internal resonances.
[Contact: Samuel P. Benz, (303) 497-5258]

DeGroot, D.C., Beall, J.A., Marks, R.B., and Rudman, D.A., **Tunable Microwave Properties of $YBa_2Cu_3O_{7-\delta}$ $SrTiO_3$ Thin Film Transmission Lines**.

[See Microwave and Millimeter-Wave Metrology.]

Doderer, T., Lachenmann, S.G., Huebener, R.P., Booi, P.A.A., and Benz, S.P., **Direct Observation of Vortex Dynamics In Two-Dimensional Josephson Junction Arrays**, to be published in the IEEE Transactions on Applied Superconductivity, Proceedings of the Applied Superconductivity Conference, Boston, Massachusetts, October 16-21, 1994.

Spatially resolved images of the dynamic states of current-biased overdamped two-dimensional arrays of $Nb/AlO_x/Nb$ Josephson junctions were obtained using low-temperature scanning electron microscopy. We present two-dimensional imaging results combined with model calculations describing various vortex dynamic regimes. The nucleation of current-induced vortices at the array boundaries and their subsequent motion into the array interior is observed for bias currents slightly above the array critical current. Vortex-vortex interaction becomes important when the bias current is increased. Conclusions on the coherent microwave radiation emission are presented.
[Contact: Samuel P. Benz, (303) 497-5258]

Eckstein, J.N., Bozovic, I., Virshup, G.F., Ono, R.H., and Benz, S.P., **Stacked Series of High-T_c Trilayer Josephson Junctions**.

We report on the properties of stacked series arrays of trilayer Josephson junctions grown by atomic layer-by-layer molecular beam epitaxy. Trilayer Josephson junctions oriented so that the current travels in the c-axis direction have been described previously. Series arrays are made by placing more than one barrier layer in the BSCCO-based epitaxial structure. Single molecular layers of BSCCO-2212 doped with Dy to reduce the local carrier concentration are used as barriers, and are placed very closed to each other, e.g., separated by only a few molecular layers of the superconducting phase. Phase locking of ac Josephson currents has been observed. The critical current density of such junctions has been observed to be very uniform on wafers that are free of second-phase defects, and operation up to 60 K has been obtained.
[Contact: Ronald H. Ono, (303) 497-3762]

Ekin, J.W., Russek, S.E., Clickner, C.C., and Sanders, S.C., **Oxygen Annealing Characteristics for Ex-Situ YBCO/Ag Thin-Film Interfaces**.

A rapid thermal annealing apparatus was used to measure the interface resistivity of YBCO/Ag interfaces at different oxygen annealing temperatures for a series of ex-situ fabricated thin-film contacts having sizes ranging from 16 μm x 16 μm down to 2 μm x 2 μm. The interface resistivity began to decrease after annealing at 300 ^{o}C for 10 min. in one atmosphere oxygen. After annealing at 400 ^{o}C, contact resistivity decreased by several orders of magnitude to the 10^{-7} Ω-cm^2 range. The 500 nm thick Ag layer showed massive diffusion and balling up for annealing temperatures above 400 ^{o}C; this temperature thus represents a practical limit for oxygen annealing the YBCO/Ag interface system. Rapid cooling of the chip after annealing led to a severe loss of critical current density in the YBCO layer, which could be restored by reannealing and cooling at a slower rate of 50 ^{o}C/min. The relative shape of the conductance vs voltage characteristics of the YBCO/Ag interface was essentially unaltered by oxygen annealing; the overall parabolic shape, superconducting gap features, and magnetic-scattering zero bias anomaly remained constant, even though the contact conductance increased by several orders of magnitude. These data suggest that Ag diffusion, not oxygen diffusion, is responsible for the decrease in interface conductivity with annealing.
[Contact: John W. Ekin, (303) 497-5448]

Grossman, E.N., Vale, L.R., Rudman, D.A., Zink,

L.R., and Evenson, K.M., **30 THz Mixing Experiments on High Temperature Superconducting Josephson Junctions**.

We have examined various properties of high-characteristic frequency $YBa_2Cu_3O_{7-\delta}$ superconductor-normal-superconductor Josephson junctions that are important to their performance as THz bandwidth mixers. We have directly observed (2nd order) beat notes at frequencies from 10 MHz to 12.8 GHz. Applying a third microwave signal to the junction, we have observed beat notes up to 27 GHz. The dc bias dependence of the beat note, and other evidence, suggests two distinct mixing mechanisms: hot-electron mixing in the junction banks at high-dc biases, and bolometric Josephson mixing at low-dc biases. The latter is the first observation of Josephson mixing at CO_2 laser frequencies in high-T_c junctions. The Josephson mixing has generated observable mixing products up to 6th order.
[Contact: Erich N. Grossman, (303) 497-5102]

Irwin, K.D., Nam, S.W., Cabrera, B., Chugg, B., Park, S.G., Welty, R.P., and Martinis, J.M., **A Self-Biasing Cryogenic Particle Detector Utilizing Electrothermal Feedback and a SQUID Readout**.

We are developing and testing a new type of superconducting transition edge sensor for phonon-mediated particle detection. This sensor consists of a superconducting tungsten thin film deposited on a silicon substrate. The temperature of the film is held constant within the superconducting transitions (T_c = 70 mK) by a feedback process, with the substrate temperature well below the film temperature. Phonon energy deposited in the film is removed by a reduction in feedback Joule heating, which is measured using a series array of DC SQUIDs. The resulting signals show improvements in linearity and signal-to-noise ratio over our previous transition edge sensors.
[Contact: John M. Martinis, (303) 497-3597]

Kautz, R.L., **Phase Locking in Two-Dimensional Josephson Junction Arrays: Effect of Critical-Current Nonuniformity**.

Numerical simulations are used to study mutual phase locking in two-dimensional arrays of Josephson junctions for parameters typical of successful millimeter-wave oscillators. Such arrays are shown to be very tolerant of random critical-current nonuniformities. However, comparison with an equivalent series array reveals that the locking between rows in a two-dimensional array is principally due to feedback through the external load and not to internal coupling between rows.
[Contact: Richard L. Kautz, (303) 497-3391]

Lachenmann, S.G., Doderer, T., Hilbert, F., Huebener, R.P., Booi, P.A.A., and Benz, S.P., **Novel Vortex Dynamics in Two-Dimensional Josephson Arrays**, to be published in the Proceedings of the Nonlinear Superconducting Devices and High-T_c Materials Conference, Capri, Italy, October 8-13, 1994.

We present spatially resolved studies of vortex dynamics in two-dimensional Josephson-junction arrays. For bias currents smaller than the array critical current, a small local thermal perturbation at the array boundaries lowers the vortex entry barrier and the array switches to the resistive state. For bias currents slightly above the array critical current, vortices and antivortices are nucleated at opposite edges of the array. An alternating crossing vortex motion is observed experimentally.
[Contact: Samuel P. Benz, (303) 497-5258]

Missert, N.N., Vale, L.R., Ono, R.H., Reintsema, C.D., Rudman, D.A., Thomson, R.E., and Berkowitz, S.J., **Temperature Dependence and Magnetic Field Modulation of Critical Currents in Step-Edge SNS YBCO/Au Junctions**.

We compare the electrical transport properties of superconductor-normal metal-superconductor (SNS) step-edge YBCO/Au junctions where the Au is deposited at 100 °C and 600 °C. For both types of junctions, we observe resistively shunted junctions current-voltage characteristics. The critical currents I_c in all cases are similar for a given YBCO thickness to step height ratio, while the normal resistance R_n for the Au deposited at 600 °C is consistently 25% lower. The normalized temperature dependence of the I_cR_n product is identical for all junctions with Au deposited at high temperatures and varies among junctions on a single chop for Au deposited at 100 °C. Low magnetic field modulation of the critical current can show either the

expected Fraunhoffer-like pattern or a double-junction modulation for both types of devices. The modulation period is consistently a factor of three lower for the high-temperature deposited Au.
[Contact: Leila L. Vale, (303) 497-5121]

Ono, R.H., Reintsema, C.D., Barnes, G., Borcherdt, L., Harvey, T.E., Kunkel, G., Rudman, D.A., Vale, L.R., Missert, N., and Rosenthal, P.A., **The Critical Current and Normal Resistance of High-T_c Step-Edge SNS Junctions**.

We have fabricated high-T_c superconductor-normal metal-superconductor (SNS) Josephson junctions with a variety of controlled geometries and measured the resulting dependences of critical current and normal resistance. These studies show that we can adjust our junction parameters over orders of magnitude, thus allowing us to tailor the junctions for a variety of applications.
[Contact: Ronald H. Ono, (303) 497-3762]

Roshko, A., Russek, S.E., Trott, K.A., Sanders, S.C., Johansson, M.E., Martens, J.S., and Zhang, D., **Effects of Etching on the Morphology and Surface Resistance of $YBa_2Cu_3O_{7-\delta}$ Films**.

The surface morphology and surface resistance of sputtered $YBa_2Cu_3O_{7-\delta}$ films both before and after etching have been examined. Six different etchants were used: citric acid, nitric acid, Br-methanol, EDTA, disodium EDTA, and ion milling. The surface morphologies of the films were examined by reflection high-energy electron diffraction (RHEED) and atomic force microscopy (AFM), both before and after etching. The surface resistance (R_s) was measured at 94 GHz using a confocal resonator. An amorphous layer was found on the film surfaces after exposure to air. A few of the etches restored some of the surface crystallinity, but most caused increases in the overall surface roughness. Several of the wet etches attacked dislocations. Ion milling caused the largest degradation of surface crystallinity and a corresponding increase in R_s. Most of the chemical etches increased R_s by less than 15%.
[Contact: Alexana Roshko, (303) 497-5420]

Sanders, S.C., Russek, S.E., Clickner, C.C., and Ekin, J.W., **Evidence for Tunneling and Magnetic Scattering at In Situ YBCO/Noble-Metal Interfaces**.

We report low-temperature conductance data for in-situ $YBa_2Cu_3O_{7-\delta}$ (YBCO)/Ag, YBCO/Au, and YBCO/Pt planar c-axis interfaces. Analysis of the conductance data for these interfaces, which have resistivities as low as 1×10^{-8} Ω cm^2, indicates that tunneling is the predominant transport mechanism. Zero-bias conductance peaks are present for all of the in-situ interfaces. These peaks are analyzed in the framework of the Appelbaum model and are attributed to the presence of isolated magnetic spins at the interface. The presence and similarity of the peaks for each noble-metal overlayer supports the hypothesis that the magnetic spins are inherent to the YBCO surface.
[Contact: Steven C. Sanders, (303) 497-5096]

Sauvageau, J.E., Booi, P.A.A., Cromar, M.W., Benz, S.P., Burroughs, C.J., and Koch, J.A., **Superconducting Integrated Circuit Fabrication Process Utilizing Low-Temperature ECR-Based PECVD SiO_2 Dielectric Films**, to be published IEEE Transactions on Applied Superconductivity, Proceedings of the Applied Superconductivity Conference, Boston, Massachusetts, October 16-21, 1994.

[See Microfabrication Technology.]

Thomson, R.E., Moreland, J., and Roshko, A., **Five Distinct Methods for Surface Modification of YBCO Thin Films with the Scanning Tunneling Microscope**.

We have investigated using the scanning tunneling microscope (STM) as a tool for surface modification of YBCO thin films, and have developed five distinct methods whereby the STM tip can modify the superconductor surface. 1) By lowering the tunneling resistance, we make the tip scratch or "mill" the sample surface physically. 2) By increasing the bias voltage above about 4 Vs, we can modify the surface by what may be an electron-beam-damaging process. 3) By increasing the bias voltage above 10 V and raising the tunneling current, we can cause a different effect which probably is due to a thermal process. 4) By operating the STM in a damp carbon dioxide atmosphere, we can make the STM tip etch the surface electrochemically. 5) Finally, we have

evidence that the high-field under an extremely sharp tip displaces the oxygen atoms in the YBCO lattice. Examples of each of these techniques are shown and discussed.
[Contact: Ruth E. Thomson, (303) 497-3141]

Cryoelectronic Metrology

Recently Published

Berkowitz, S.J., De Obaldia, E., Ludwig, K.F., Jr., Skocpol, W.J., Mankiewich, P.M., Ono, R.H., Beall, J.A., Vale, L.R., Rudman, D.A., O'Malley, M.L., Drabeck, L.M., and Polakos, P.A., **Increased Transition Temperature *In-Situ* Coevaporated $YBa_2Cu_3O_{7-\delta}$ Thin Films by Low Temperature Post-Annealing**, Applied Physics Letters, Vol. 65, No. 12, pp. 1587-1589 (19 September 1994).

In-situ coevaporated $YBa_2Cu_3O_{7-\delta}$ thin films have a slightly depressed transition temperature T_c, though they have excellent radio-frequency surface resistance characteristics. These films consistently have less orthorhombic strain than laser ablated or post-annealed films. Low-temperature (320 to 420 °C) post-annealing of in situ coevaporated films in 100 kPa of O_2 raised T_c to values as high as 91.5 K with some increase in the orthorhombic strain. All measured thin films show less variation of T_c with orthorhombic strain than does bulk material.
[Contact: Ronald H. Ono, (303) 497-3762]

Kautz, R.L., **Quasipotential and the Stability of Phase Lock in Nonhysteretic Josephson Junctions**, Journal of Applied Physics, Vol. 76, No. 9, pp. 5538-5544 (November 1994).

[See Fundamental Electrical Measurements.]

Kautz, R.L., Benz, S.P., and Reintsema, C.D., **Large-Amplitude Shapiro Steps and Self-Field Effects in High-T_c Josephson Weak Links**, Applied Physics Letters, Vol. 65, No. 11, pp. 1445-1447 (September 1994).

[See Fundamental Electrical Measurements.]

Nahum, M., Eiles, T.M., and Martinis, J.M., **Electronic Microrefrigerator Based on a Normal-Insulator-Superconductor Tunnel Junction**, Applied Physics Letters, Vol. 65, No. 24, pp. 2123-2125 (December 1994).

We present measurements on a novel electronic microrefrigerator that can cool conduction electrons significantly below the lattice temperature. A normal-insulator-superconductor tunnel junction is used to extract electrons from the normal metal electrode whose energy is higher than the Fermi energy. Electrons with an average energy equal to the Fermi energy are returned to the metal by a superconducting contact. Consequently, the high-energy thermal excitations are removed from the normal metal, thus cooling the electrons. For lattice temperatures higher than 100 mK, the data can be explained by a simple theory incorporating the BCS density of states in the superconducting electrode and the coupling between electrons and phonons. At lower temperatures, our measurement suggests that the electron energies in the normal electrode depart strongly from an equilibrium distribution.
[Contact: John M. Martinis, (303) 497-3597]

Rice, J.P., Grossman, E.N., and Rudman, D.A., **Antenna-Coupled High-T_c Air-Bridge Microbolometer on Silicon**, Applied Physics Letters, Vol. 65, No. 6, pp. 773-775 (August 1994).

An antenna-coupled high-T_c superconducting microbolometer on a silicon substrate, operating at infrared wavelengths, is described. This detector incorporates a silicon-micromachined yttria-stabilized zirconia air bridge at the feed of a planar lithographic antenna to simultaneously minimize the thermal conductance and the heat capacity of the bolometer. At an operating temperature of 87.4 K, the optical responsivity measured using a 300-K blackbody source over a 0.2- to 2.9-THz bandwidth is 2900 V/W, the optical noise-equivalent power (NEP) is 9×10^{-12} W/Hz$^{1/2}$, and the time constant is <10 μs. This NEP is nearly a factor of 2 lower than the previous record for a liquid-nitrogen-cooled thermal detector, and the time constant is several orders of magnitude shorter.
[Contact: Joseph P. Rice, (303) 497-7366]

Sanders, S.C., Russek, S.E., Clickner, C.C., and Ekin, J.W., **Insulating Boundary Layer and Magnetic Scattering in $YBa_2Cu_3Y_{7-\delta}$/Ag Interfaces over a Contact Resistivity Range of 10^{-8}-10^{-3} Ω-cm^2**, Applied Physics Letters, Vol. 65, No. 17 pp. 2232-2234 (24 October 1994).

We have measured interface transport in thin-film $YBa_2Cu_3O_{7-\delta}$/Ag interfaces having resistivities ranging from 10^{-8} to 10^{-3} Ω-cm^2. Analysis of the interface I-V data indicates that tunneling is the predominant transport mechanism even for the in-situ interfaces having contact resistivities of 1 to 7 × 10^{-8} Ω-cm^2. Zero-bias conductance peaks are also observed for the entire range of interface resistivity. The similarity of the zero-bias conductance peaks among these widely varying interfaces suggests that the low-temperature interface transport is governed by the same mechanism in each case. These conductance peaks are analyzed in the framework of the Appelbaum-Anderson model for tunneling assisted by magnetic scattering from isolated magnetic spins in the interface.
[Contact: Steven C. Sanders, (303) 497-5096]

Thomson, R.E., Moreland, J., and Roshko, A., **Surface Modification of $YBa_2Cu_3O_{7-\delta}$ Thin Films Using the Scanning Tunneling Microscope: Five Methods**, Nanotechnology, Vol. 5, pp. 57-69 (1994).

We have investigated using the scanning tunneling microscope (STM) as a tool for surface modification of $YBa_2Cu_3O_{7-\delta}$ (YBCO) thin films, and have identified five distinct methods whereby the STM tip can modify the superconductor surface. 1) By lowering the tunneling resistance, we make the tip scratch or "mill" the sample surface mechanically. 2) By increasing the bias voltage above about 4 V, we can modify the surface by an apparent electron-beam-damaging process. 3) By increasing the bias voltage above 10 V and raising the tunneling current, we can cause a more dramatic effect which is probably due to a thermal process. 4) By operating the STM in a damp carbon dioxide atmosphere, we can cause the STM tip to etch the surface electrochemically. 5) Finally, we have some preliminary date suggesting that the high field under an extremely sharp tip displaces the oxygen atoms in the YBCO lattice. Examples of each of these techniques are shown and discussed.
[Contact: Ruth E. Thomson, (303) 497-3141]

Wiesenfeld, K., Benz, S.P., and Booi, P.A.A., **Phase-Locked Oscillator Optimization for Arrays of Josephson Junctions**, Journal of Applied Physics, Vol. 76, No. 6, pp. 3835-3846 (15 September 1994).

An overview of phase locking in two-dimensional (2D) arrays of identical Josephson junctions is presented. General design criteria are discussed for optimization of power and linewidth. A harmonic balance technique is used to derive an analytic expression for the fundamental power as a function of bias voltage for a single shunted-tunnel junction with an external shunt resistor having parasitic inductance. A linear stability analysis is performed on the in-phase state of 2D arrays in the absence of any external load. Most excitation modes in the 2D array are damped, leading to stable phase locking between parallel junctions within each row; however, within the theoretical model, no mechanisms intrinsic to the array were found to induce phase locking between rows of junctions. The results of these calculations and their impact on and relevance to the design of phase-locked Josephson oscillators are discussed.
[Contact: Samuel P. Benz, (303) 497-5258]

Antenna Metrology

Released for Publication

Francis, M.H., Kremer, D.P., Jacobson, M.D., Fedor, L.S., Hazen, D.A., and Madsen, W.B., **A Dual-Frequency Millimeter-Wave Radiometer Antenna for Airborne Remote Sensing of Atmosphere and Ocean**, to be published in Proceedings of the Antenna Measurement Techniques Association Symposium, Long Beach, California, October 3-7, 1994.

Accurate multiwavelength radiometric remote sensing of the ocean and the atmosphere from an aircraft requires antennas with the same beamwidth at the various frequencies of operation. Scientists at the National Oceanic and Atmospheric Administration designed an offset antenna with a pressure-compensating corrugated feed horn to meet this criterion. A specially designed fairing was incorporated into the antenna to optimize the aerodynamics and minimize the liquid buildup on the antenna surfaces. The antenna has two positions: the zenith (up) position and the nadir (down) position. The planar near-field facility at the National Institute of Standards and Technology was used to determine the far-field pattern of the antenna. The results show that the antenna beamwidths at 23.87 and 31.65 GHz are nearly the same as expected from

the design criterion. This antenna was recently used in an ocean remote-sensing experiment and performed according to expectations.
[Contact: Michael H. Francis, (303) 497-5873]

Guerrieri, J.R., and Tamura, D.T., **Accurate Insertion Loss Measurement for Near-Field Antenna Testing**, to be published in the Proceedings of the Antenna Measurement Techniques Association Symposium, Long Beach, California, October 3-7, 1994.

Absorber material is used in antenna measurements to reduce multiple reflections and multipath. However, in some cases this absorber can still have an uncertainty larger than the desired uncertainty of the measurement.

For accurate antenna gain measurements, using the planar, cylindrical and spherical near-field methods, insertion loss measurements should be accurate to within +0.03 dB. To satisfy this requirement, it is important to minimize the multiple reflections between the probe and antenna under test. If the multiple reflections are too large, then the insertion loss becomes very position sensitive, and errors on the order of a decibel can be introduced. It is imperative that absorber be used to cover all metal surfaces. Errors can also be introduced if the absorber is not used carefully. The effects on antenna gain data measured with and without absorber are shown. Measurement results showing the effect of the placement of the absorber on the antenna under test are also presented. This includes absorber distance from the antenna's aperture, the rotation of absorber about the antenna's coordinate system, and the use of different types of absorber.
[Contact: Jeff Guerrieri, (303) 497-3863]

Lewis, R.L., **Spherical-Wave Source-Scattering Matrix Analysis of Antennas and Antenna-Antenna Interactions**, to be published as NIST Technical Note 1373.

Expressions are presented for describing incoming and outgoing fields about an antenna in terms of a series of exciting and emergent vector spherical-wave functions. The exciting and emergent fields around the antenna's exterior are related to the field in the antenna feed via a source-scattering matrix representation. A series of so-called spherical-wave source-scattering matrix coefficients are then related to more conventional parameters such as antenna gain and receiving cross section. An overview of rotation and translation theorems for transforming vector spherical-wave functions between two distinct coordinate systems is given, followed by a general solution to the problem of expressing the coupling between two coupled antennas in terms of each antenna's spherical-wave source-scattering matrix representation. We go on to consider special results to substantiate our formulation, such as showing equivalence between the coupling equations for transmission in opposite directions when the antennas are reciprocal, showing uniform convergence of some series representations for antenna coupling and simultaneously obtaining a coordinate-system translation theorem for the dyadic Green's function, and lastly showing that our two-antenna coupling equations reduce to expressions for the incident and emergent fields about a single antenna when the other antenna is an elementary dipole. Efficient probe-corrected spherical and hemispherical scanning algorithms are then developed for processing measured near-field data to obtain antenna's far-field pattern. Finally, we describe a number of self-consistency tests and theoretical-data simulations that were developed to validate our spherical-scanning algorithm, and we describe an independent experimental verification.
[Contact: Richard L. Lewis, (303) 497-5196]

Antenna Metrology

Recently Published

Francis, M.H., Newell, A.C., Grimm, K.R., Hoffman, J., and Schrank, H.E., **Planar Near-Field Measurements of Low-Sidelobe Antennas**, Journal of Research of the National Institute of Standards and Technology, Vol. 99, No. 2, pp. 143-167 (March—April 1994). [Also published in the Proceedings of the 15th Annual Meeting and Symposium, Antenna Measurement Techniques Association, Dallas, Texas, October 4-8, 1993, pp. 184-190.]

The planar near-field measurement technique is a proven technology for measuring ordinary antennas operating in the microwave region. The develop-

ment of very low-sidelobe antennas raises the question whether this technique can be used to accurately measure these antennas. We show that data taken with an open-end waveguide probe and processed with the planar near-field methodology, including probe correction, can be used to accurately measure the sidelobes of very low-sidelobe antennas to levels of -55 to -60 dB relative to the main beam peak. A special probe with a null in the direction of the main beam was also used for some of these measurements. This special probe reduced some of the measurement uncertainties, but increased the uncertainties due to probe-antenna interactions. We discuss the major sources of uncertainty and show that the probe-antenna interaction is one of the limiting factors in making accurate measurements. The test antenna for this study was a slotted-waveguide array whose low sidelobes were known. The near-field measurements were conducted on the NIST planar near-field facility.
[Contact: Michael H. Francis, (303) 497-5873]

Jacobson, M.D., Fedor, L.S., Hazen, D.A., Madsen, W.B., Francis, M.H., and Kremer, D.P., **A Dual Frequency mm-Wave Radiometer Antenna for Airborne Remote Sensing of Atmosphere and Ocean**, Microwave Journal, Vol. 27, No. 9, pp. 24-38 (September 1994).

Accurate multiwavelength radiometric remote sensing of the ocean and the atmosphere from an aircraft requires antennas with the same beamwidth at the various frequencies of operation. An offset antenna was designed with a pressure-compensating corrugated feed horn to meet this criterion. A specially designed fairing was incorporated into the antenna to optimize the aerodynamics and minimize the liquid build-up on the antenna surfaces. The antenna has two positions, the zenith (up) position and the nadir (down) position. The far-field pattern results show that the antenna beamwidths at 23.87 and 31.65 GHz agree well with design criterion. This antenna was recently used in an ocean remote-sensing experiment and performed according to expectations.
[Contact: Michael H. Francis, (303) 497-5873]

Lewis, R.L., Muth, L.A., and Wittmann, R.C., **RangeCAD and the NIST RCS Uncertainty Analysis**, NISTIR 5022 (August 1994).

We discuss the salient features of a computer program, RangeCAD, and then translate the program's output into a catalog of radar cross-section (RCS) uncertainties. This specific catalog was developed by NIST to standardize RCS uncertainty computations at the various RCS measurement sites. We check uncertainty estimates generated by RangeCAD against alternative formulations that approximate equivalent uncertainty specifications. Based on this comparison, we conclude that the uncertainty estimates generated by RangeCAD provide realistic values for the NIST RCS uncertainty analysis.
[Contact: Richard L. Lewis, (303) 497-5196]

Noise Metrology

Released for Publication

Clark, A.F., and Steiner, R.L., **Noise Characteristics Below 1 Hz of Zener Diode-Based Voltage References**, to be published an Abstract in the Bulletin of the American Physical Society Meeting, San Jose, California, March 13-17, 1995.

[See DC and Low-Frequency Metrology.]

Noise Metrology

Recently Published

Pucic, S.P., **Uncertainties of the NIST Coaxial Noise Calibration System**, Digest of the 1994 Conference on Precision Electromagnetic Measurements, Boulder, Colorado, June 27—July 1, 1994, pp. 254-255.

Uncertainties of the NIST broadband coaxial calibration system are analyzed. The expanded relative uncertainty for a source with the ENR of $\approx$15 dB is typically 1.6%.
[Contact: Sunchana P. Pucic, (303) 497-3546]

Wait, D.F., **Relative Accuracy of Isolated and Unisolated Noise Comparison Radiometers**, Digest of the 1994 Conference on Precision Electromagnetic Measurements, Boulder, Colorado, June 27—July 1, 1994, pp. 256-257.

A rigorous radiometer equation is derived and used to develop better corrections and uncertainty

estimates. Isolated and well-corrected unisolated radiometers have similar accuracies for low reflection coefficient sources. To ignore corrections for the finite isolation of a radiometer, about 38-dB isolation is needed.
[Contact: David F. Wait, (303) 497-3610]

Microwave and Millimeter-Wave Metrology

Released for Publication

DeGroot, D.C., Beall, J.A., Marks, R.B., and Rudman, D.A., **Tunable Microwave Properties of $YBa_2Cu_3O_{7-\delta}$ $SrTiO_3$ Thin Film Transmission Lines**.

Monolithic microwave circuits with low-signal losses and voltage-tunable properties can be produced by integrating the advantages of high-temperature superconductor and ferroelectric thin films. To explore the electrical characteristics of such devices, we fabricated a series of copolar waveguide transmission lines of varying geometries in laser-deposited $YBa_2Cu_3O_{7-\delta}$ and $SrTiO_3$ thin films. We characterized the two-port microwave response and voltage tunable properties of the transmission lines at cryogenic temperatures using a calibrated network analyzer system. Total phase shifts and phase tuning in these devices increased by large factors for increasing ferroelectric film thickness. A tri-layer configuration, with $SrTiO_3$ layers on both sides of the $YBa_2Cu_3O_{7-\delta}$ film, produced substantially larger delays and changes in phase shift than bi-layer devices. Since transmission losses increased only moderately with ferroelectric inclusion, this study identifies a range of device geometries that produce technologically important phase tuning with small signal losses.
[Contact: Donald C. DeGroot, (303) 497-7212]

Hayden, L.A., Marks, R.B., and Rettig, J.B., **Accuracy and Repeatability in Time Domain Network Analysis**, to be published in the Proceedings of Automatic Radio Frequency Techniques Group, Boulder, Colorado, December 1-2, 1994.

This paper examines the importance of measurement repeatability in time domain network analysis and includes an analysis of the limitations imposed on theoretical accuracy by measurement noise. A closed-loop correction algorithm implemented in a fast, equivalent-time sampling, time domain reflectometer improves source timing accuracy, the dominant cause of nonrepeatability. An example measurement of attenuation in a 3.5-mm coaxial airline demonstrates performance approaching this theoretical noise limit and the limits imposed by connector repeatability.
[Contact: Roger B. Marks, (303) 497-3037]

Marks, R.B., and Williams, D.F., **Accurate Electrical Characterization of High-Speed Interconnections**, to be published in the Proceedings of the 27th International Symposium on Microelectronics, Boston, Massachusetts, November 15, 1994.

A program at the National Institute of Standards and Technology supports the electrical characterization of electronic packaging and interconnections in terms of scattering parameters, impedances, and transmission line parameters. This paper reviews the basic methodology, including its origins in the characterization of monolithic microwave integrated circuits, and describes the resulting calibration and measurement methods that have been developed.
[Contact: Roger B. Marks, (303) 497-3037]

Marks, R.B., and Williams, D.F., **Comments on "Conversions Between S, Z, Y, h, ABCD, and T Parameters Which Are Valid for Complex Source and Load Impedance."**

A recently published paper [D.A. Frickey, IEEE Trans. Microwave Theory Tech., vol. 42, pp. 205-211, Feb. 1994], presents formulas for conversions between various network matrices. However, these parameters are defined using an unconventional definition of the waves and therefore yield unexpected results.
[Contact: Roger B. Marks, (303) 497-3037]

Williams, D.F., and Marks, R.B., **Compensation for Substrate Permittivity in Probe-Tip Calibration**, to be published in the Proceedings of the Automatic Radio Frequency Techniques Group, Boulder, Colorado, December 1-2, 1994.

We demonstrate a method of compensation for the effect of substrate permittivity on coplanar waveguide probe-tip scattering parameter calibra-

tions, modeling the effect as a capacitance at the probe tip. Comparison to on-wafer multiline TRL calibration verifies its accuracy. The method allows calibration to the probe tip using generic off-wafer standards with accuracy comparable to that of on-wafer calibration.
[Contact: Dylan F. Williams, (303) 497-3138]

Electromagnetic Properties

Released for Publication

Baker-Jarvis, J.R., and Janezic, M.D., **Analysis of a Two-Port Flanged Coaxial Holder for Shielding Effectiveness and Dielectric Measurements of Thin Films and Thin Materials**.

A two-port flanged coaxial probe for measuring the dielectric and magnetic properties of thin material sheets is analyzed. Closed form solutions for the two-port scattering parameters are presented. The solution assumes an incident TEM wave together with evanescent TM_{0n} modes. Numerical results are obtained for both the forward and inverse problem. Computations indicate that at low frequencies the incident waves are almost totally reflected. As the frequency is increased, transmission through the sample increases. Experimental results compare closely with theory. The inverse solution yielded good permittivity determination for the cases tested. The technique should prove useful for nondestructive testing of circuit boards or substrates.
[Contact: James-Baker Jarvis, (303) 497-5621]

Galt, D., Price, J.C., Beall, J.A., and Harvey, T.E., **Ferroelectric Thin Film Characterization Using Superconducting Microstrip Resonators**.

We describe a novel technique for characterizing the dielectric response of ferroelectric thin films at microwave frequencies. The method involves a microstrip resonator which incorporates a ferroelectric capacitor at its center. To demonstrate this method, we have fabricated a superconducting microstrip resonator from a laser ablated $YBa_2Cu_3O_{7-\delta}$ film on a $LaAlO_3$ (LAO) substrate with a $SrTiO_3$ (STO) capacitor at its center. We report the observed dielectric behavior of the STO laser-ablated film as a function of bias at liquid He and N_2 temperatures and at high and low frequencies. It is observed that the electrically tunable dielectric constant of the STO film is roughly independent of frequency up to 20 GHz (especially at high bias). The loss tangent of the STO/LAO capacitor decreases with increasing bias and is apparently independent of frequency between 6 and 20 GHz.
[Contact: James A. Beall, (303) 497-5989]

Geyer, R.G., Krupka, J., Kuhn, M., and Hinken, J., **Dielectric Properties of Single Crystals of Al_2O_3, $LaAlO_3$, $NdGaO_3$, $SrTiO_3$, and MgO at Cryogenic Temperatures**, IEEE Transactions on Microwave Theory and Techniques, Vol. 42, No. 10, pp. 1886-1890 (October 1994).

A dielectric resonator technique has been used for measurements of the permittivity and dielectric loss tangent of single-crystal dielectrics in the temperature range 20 to 300 K at microwave frequencies. Application of superconducting films made it possible to determine dielectric loss tangents of about 5×10^{-7} at 20 K. Two permittivity tensor components for uniaxially anisotropic samples were measured. Generally, single-crystal samples made of the same material by different manufacturers or by different processes have significantly different losses, although they have essentially the same permittivities. The permittivity of one crystalline ferroelectric substrate, $SrTiO_3$, strongly depends on temperature. This temperature dependence can affect the performance of ferroelectric thin-film microwave devices, such as electronically tunable phase shifters, mixers, delay lines, and filters.
[Contact: Richard G. Geyer, (303) 497-5852]

Jones, C.A., **Substrate and Thin Film Measurements**, to be published in the Proceedings of the 1994 Wireless Circuits, Interconnection, and Assembly Workshop, Phoenix/Scottsdale/-Chandler, Arizona, October 16-19, 1994.

This paper describes the use of cavity resonators, coaxial probes, capacitive measurements and dielectric resonators for characterizing the electromagnetic properties of substrates and thin films. Cavity resonators are typically capable of accurately measuring materials having dielectric losses ($\tan \delta$) less than 1×10^{-3}. Coaxial probes are useful for nondestructive measurements and are often preferred in industrial applications. However, the use coaxial probes for substrate permittivity (ϵ_r^*)

measurements is affected by the presence of an effective air gap, due to surface roughness, between the sample under test and the probe. Capacitive measurements also suffer from the same effective air gap; therefore, permittivity measurement results have an uncertainty of 2 to 10 percent, provided $\epsilon_r' < 10$. Measurement of substrate materials with dielectric resonators is a very accurate method for characterization of low-loss dielectric materials. Dielectric resonators are capable of uncertainties to within 0.3%, provided $\epsilon_r' < 35$. The major drawback for this technique is that the substrate material must be precisely machined into a cylindrical sample.
[Contact: Chriss A. Jones, (303) 497-5958]

Mantese, J.V., Micheli, A.L., Dungan, D.F., Geyer, R.G., Baker-Jarvis, J., and Grosvenor, J., **Ferroelectric/Ferrimagnetic Composites with Composition Dependent Permittivities and Permeabilities - Comparison with Effective Medium Theory**.

High-frequency (1 MHz - GHz) transmission line analysis was used to determine the frequency-dependent complex permittivities and complex permeabilities of ferroelectric/ferrimagnetic (barium titanate and a magnesium-copper-zinc ferrite) composites. The effective medium rules of Maxwell-Garnett give both lower and upper bounds for the effective permittivities and permeabilities and yield accurate estimates of the bulk electric and magnetic properties at low-volume fill fraction of either component provided the proper host matrix is chosen. Bruggeman theory, however, yielded the best predictive values for the permittivity and permeability over the entire composition range with the observed microstructure most consistent with this formalism.
[Contact: Richard G. Geyer, (303) 497-5852]

Electromagnetic Properties

Recently Published

Baker-Jarvis, J., and Janezic, M.D., **Distribution of Dielectric Relaxation Times and the Moment Problem**, Digest of the 1994 Conference on Precision Electromagnetic Measurements, Boulder, Colorado, June 27—July 1, 1994, pp. 356-357.

A procedure for deconvolving time-dependent distribution functions from permittivity data is developed. The problem is reduced to solving an associated moment problem using a maximum-entropy procedure. The method is applied to synthetic permittivity modeling, both for in-band and out-of-band regions. The numerical results indicate that the technique has potential for deconvolving the distribution function from the permittivity data.
[Contact: James Baker-Jarvis, (303) 497-5621]

Baker-Jarvis, J., and Janezic, M.D., **Open-Ended Coaxial Probes for Nondestructive Testing of Substrates and Circuit Boards**, Proceedings of the Materials Research Society Symposium, Vol. 347, pp. 215-220 (1994).

The results of the full-wave model theory for the open-ended coaxial probe with lift-off are presented and are applied to measurements of thin materials. The model allows the study of the open-ended coaxial probe as a nondestructive testing tool. The equations presented are valid for both dielectric and magnetic materials. The analysis yields insight into the effects of air gaps on probe measurements. Numerical results indicate that the probe is very sensitive to lift-off at low frequencies. This sensitivity decreases somewhat as frequency increases. In order for the field to penetrate the air gap, larger size coaxial line or higher frequencies need to be used. An application of the theory is performed by numerically solving the inverse problem using measured reflection coefficient.
[Contact: James Baker-Jarvis, (303) 497-5621]

Baker-Jarvis, J., Janezic, M.D., Domich, P.D., and Geyer, R.G., **Analysis of an Open-Ended Coaxial Probe with Lift-Off for Nondestructive Testing**, IEEE Transactions on Instrumentation and Measurement, Vol. 43, No. 5, pp. 711-718 (October 1994).

The open-ended coaxial probe with lift-off is studied using a full-wave analysis, and an uncertainty analysis is presented. The field equations for the following terminations are worked out: (1) the sample extends to ∞ in the positive axial direction; (2) the sample is backed by a well-characterized material; and (3) the sample is backed by a short-circuit termination. The equations are valid for both dielectric and magnetic materials. The model

allows the study of the open-ended coaxial probe as a nondestructive testing tool. The analysis allows a study of the effects of air gaps on probe measurements. The reflection coefficient and phase are studied as a function of lift-off, coaxial line size, permittivity, permeability, and frequency. Numerical results indicate the probe is very sensitive to lift-off. For medium to high-permittivity values and electrically small probes, gaps on the order to fractions of a millimeter strongly influence the reflection coefficient. In order for the field to penetrate through the air gap, larger size coaxial line or higher frequencies need to be used. A comparison of the theory to experiment is presented. The results are in close agreement. A differential uncertainty analysis is also included.
[Contact: James Baker-Jarvis, (303) 497-5621]

Geyer, R.G., and Krupka, J., **Dielectric Properties of Materials at Cryogenic Temperatures and Microwave Frequencies**, Digest of the 1994 Conference on Precision Electromagnetic Measurements, Boulder, Colorado, June 27—July 1, 1994, pp. 350-351.

The permittivity and dielectric loss tangent of single-crystal quartz, cross-linked polystyrene (Rexolite), and polytetrafluoroethylene (Teflon) were measured at microwave frequencies and at temperatures of 77 K and 300 K using a dielectric resonator technique. Application of high-temperature superconducting films as the endplates of the dielectric resonator made it possible to determine dielectric loss tangents of about 7×10^{-6} at 77 K. Two permittivity tensor components for uniaxially anisotropic crystalline quartz were measured. Although the permittivities at 77 K changed very little from their room temperature values at 300 K, large changes in dielectric losses were observed. The decreased loss characteristics of these microelectronic substrates can markedly improve the performance of many microwave devices at cryogenic temperatures.
[Contact: Richard G. Geyer, (303) 497-5852]

Geyer, R.G., Mantese, J., and Baker-Jarvis, J., **Effective Medium Theory for Ferrite-Loaded Materials**, NIST Technical Note 1371 (October 1994).

A ferrite-loaded composite medium is modeled by spherical inclusions spaced equally on a cubic lattice within a host matrix. Both the inclusions and host matrix may be magnetically permeable and possess dielectric and magnetic loss. The ferrite-loaded medium may be considered to consist of excited Hertzian electric and magnetic dipole sources. Effective medium rules of a modified Maxwell-Garnett form can be derived by analysis of plane-wave propagation through the composite. These rules do not yield symmetric characterization of two-phase media. They are compared with other effective medium theories (Lorentz-Lorenz, Maxwell-Garnett, and Bruggeman) and broadband coaxial transmission line data measured on ferrite-loaded titanates of known composition. The modified Maxwell-Garnett rules give both lower and upper bounds for the effective permittivities and permeabilities of the composite and yield accurate estimates of bulk electric and magnetic properties for low-volumetric inclusion loading. The Bruggeman formalism yields the best predictive permittivity and permeability values when volumetric percentages of the inclusions and host matrix are approximately equal. Generally, maximal magnetic loss factors occur at a frequency where the static initial permeability decreases by a factor of one-half, and the relaxation frequency for ferrite composites increases with decreasing static initial permeability.
[Contact: Richard G. Geyer, (303) 497-5852]

Krupka, J., Geyer, R.G., and Cros, D., **Measurements of Permittivity and the Dielectric Loss Tangent of Low Loss Dielectric Materials with a Dielectric Resonator Operating on the Higher Order $Te_{0\gamma\delta}$ Modes**, Proceedings of the 10th International Microwave Conference, Mikon - 94, Książ Castle, Poland, May 30—June 2, 1994, Vol. 2, pp. 567-572.

Dielectric resonator techniques are commonly used for permittivity and the dielectric loss tangent measurements of low-loss materials. Usually, the TE_{011} mode or $TE_{01\delta}$ mode is used. In this case, if dielectric characterization is required at various frequencies, more than one sample of the material under test must be provided. These samples must have differing physical dimensions. In order to perform dielectric measurements on a single sample at several contiguous frequency subbands, higher-order $TE_{0\gamma\delta}$ modes may be utilized. These higher-order modes are tuned by changing the distance

between the conductor ground planes of the dielectric resonator. Identification of higher-order, $TE_{0\gamma\delta}$ resonant modes in several cylindrical samples of the material under test allows properties to be determined over a broad-frequency spectrum.
[Contact: Richard G. Geyer, (303) 497-5852]

Wu, H.D., Barnes, F.S., Galt, D., Price, J., and Beall, J.A., **Dielectric Properties of Thin Film $SrTiO_3$ Grown on $LaAlO_3$ with $YBa_2Cu_3O_{7-x}$ Electrodes**, Proceedings of SPIE (The International Society for Optical Engineering, P.O. Box 10, Bellingham, Washington 98227-0010), High-T_c Microwave Superconductors and Applications, Vol. 2156, pp. 131-140 (April 1994).

We have fabricated and characterized YBCO ($YBa_2Cu_3O_{7-x}$) microstrip resonators on LAO ($LaAlO_3$) substrates that include thin-film STO ($SrTiO_3$) coplanar capacitors to study the dielectric properties of thin-film STO. The low-frequency capacitance of the STO/LAO capacitor is measured as a function of temperature and dc bias. We use the observed resonant frequencies to extract the microwave frequency capacitance of the structure and the Qs to determine the microwave losses. A conformal map is developed and used to transform the observed capacitances into dielectric constant values for the thin-film STO.
[Contact: David Galt, (303) 497-5989]

Optical Fiber Metrology

Recently Published

Brilliant, N.A., and Young, M., **Video Microscopy Applied to Optical Fiber Geometry Measurements**, NIST Technical Note (November 1994).

We describe a video microscope used to measure the mean diameter and noncircularity of the cladding of optical fibers. We attempted, without success, to perform absolute measurements. When we calibrated the microscope with a fiber of known diameter; however, we could measure the cladding diameter within 0.1 μm.
[Contact: Matt Young, (303) 497-3223]

Day, G.W., Franzen, D.L., and Hickernell, R.K., Eds., **Technical Digest of the Symposium on Optical Fiber Measurements**, 1994, NIST Special Publication 864 (September 1994).

This Digest contains the manuscripts of 50 papers, 10 invited and 40 contributed, presented at the eighth Symposium on Optical Fiber Measurements, September 13-15, 1994 in Boulder, Colorado. The invited papers were selected from about 50 nominations. The contributed papers were selected from 57 submitted.

The most significant theme of the Symposium is the present importance of polarization measurements, especially polarization mode dispersion and polarization dependent loss, or the characterization of fibers and components with special polarization properties. OTDR measurements are another important theme, as they have been since the first Symposium in 1980, and the characterization of optical fiber amplifiers continues to be important. Nonlinear processes in fiber seem to be a growing interest.

Approximately two thirds of the papers come from outside of the United States, up from about half at the seventh Symposium. Ten countries are represented in the program.
[Contact: Gordon W. Day, (303) 497-5204]

Drapela, T.J., Franzen, D.L., and Young, M., **Fiber Geometry: Results of an International Interlaboratory Measurement Comparison**, in Technical Digest - Symposium on Optical Fiber Measurements, 1994, NIST Special Publication 864, G. W. Day, D. L. Franzen, and R. K. Hickernell, Eds. (September 1994), pp. 129-132.

An international measurement comparison of fiber geometry measurements showed significantly better agreement for all three fiber geometry parameters than in previous comparisons. For cladding diameter measurements, participants whose test sets were calibrated by means of a calibration artifact from one of the national standards laboratories showed significantly better agreement.
[Contact: Douglas L. Franzen, (303) 497-3346]

Patrick, H., Gilbert, S.L., and Lidgard, A., **Decrease of Fluorescence In Optical Fiber During Exposure To Pulsed or Continuous-Wave Ultraviolet Light**, chapter in Optical Materials, Vol. 3, (Elsevier Science B.V., The Netherlands

1994), pp. 209-216.

We exposed optical fibers to UV light and simultaneously measured the intensity of the blue fluorescence from the fiber core. Two silica glass fibers with different core dopants were investigated: a germanium-doped fiber and a germanium-boron-codoped fiber. The fibers were exposed transversely to pulsed or continuous-wave 244-nm light for times ranging from a few minutes to over an hour. For all UV intensities, and exposure times used, the fluorescence decreased during UV exposure. For a given fiber, the fractional decrease in fluorescence seen from the side of the fiber was dependent only on the total UV fluence. The side-collected fluorescence from the germanium-doped fiber decreased to 60% of its initial value after exposure to 3600 J/cm^2 fluence, while the fluorescence from the germanium-boron-codoped fiber decreased to 40% of its initial value after the same fluence. We compared the temporal characteristics of the fluorescence radiated transversely to the exposed region with that which was collected from the end of the fiber. The temporal characteristics of the fluorescence guided down the core and collected from the end were masked by photodarkening that occurred on the same time scale. We relate the observed fluorescence decrease to competing theories of its origin and relationship to photoinduced refractive index changes.
[Contact: Heather Patrick, (303) 497-6353]

Wang, C.M., Vecchia, D.F., Young, M., and Brilliant, N.A., **Software for Performing Gray-Scale Measurements of Optical Fiber End Faces**, NIST Technical Note 1370 (November 1994).

The video microscope, or gray-scale, method is the most frequently used technique on the manufacturing floor for measuring critical dimensions of an optical fiber end face. Gray-scale images of optical fibers and hence their corresponding edge tables, or locus of points that represent the edge of the fiber in digitized form, can easily be contaminated by dirt or distorted by faulty cleaves. Analysis of such edge tables can be difficult. We present a method for performing optical fiber dimensional quality control which allows for end-face damage and accounts for the special structure of measurement errors in fiber edge tables. The new approach adheres to the industrial standard test procedure by fitting an ellipse to the edge table to obtain geometric measurements. But to create high-breakdown resistance to outliers, a data filter based on the least-median-of-squares criterion is used. Some computational issues and a brief description of a computer program that takes the digitized image, locates and filters the edge points, and estimates the geometric parameters of interest are given. Its operation is also described.
[Contact: Matt Young, (303) 497-3223]

Optical Fiber/Waveguide Sensors

Released for Publication

Clarke, I.G., Rochford, K.B., Rose, A.H., and Day, G.W., **A Polarization Insensitive 3 x 3 Sagnac Current Sensor Using Polarizing Spun High-Birefringence Fiber**, to be published in the Proceedings of the 10th Optical Fiber Sensors Conference, Glasgow, Scotland, UK, October 11-13, 1994.

The response functions of previously reported 3 x 3 Sagnac current sensors are strongly dependent on input polarization, so systems require careful control of the input polarization state. In this paper, we describe a simple method for eliminating this polarization dependence so that stable response functions are obtained. We demonstrate the existence of wavelength range over which spun high-birefringence fiber guides only one elliptically polarized mode, thus preserving a single polarization state. Using this effect, we show that 3 × 3 Sagnac current sensor response functions can exhibit stable phase offsets with little sensitivity to input polarization. This provides practical current sensing without the need for polarization control.
[Contact: Kenneth B. Rochford, (303) 497-5170]

Optical Fiber/Waveguide Sensors

Recently Published

Deeter, M.N., Day, G.W., and Rose, A.H., **Magnetooptic Materials**, chapter in CRC Handbook of Laser Science and Technology, Supplement 2: Optical Materials, Vol. 5, M. J. Weber, Ed. (CRC Press, Inc., Boca Raton, Florida, January 1995), pp. 367-402.

We reviewed the origins and applications of various magneto-optic effects, including the Faraday and Kerr effects, and magnetic linear birefringence. Mathematically, we show how all of these effects can be derived from a single dielectric tensor. We then consider the characteristics of magneto-optic effects in specific material classes, including diamagnetic, paramagnetic, ferromagnetic, ferrimagnetic, and antiferromagnetic materials. Relevant data for each class are summarized in tabular format. Finally, both scientific and commercial applications of magneto-optic materials are described.
[Contact: Merritt N. Deeter, (303) 497-5400]

Deeter, M.N., Milián Bon, S., Day, G.W., Diercks, G., and Samuelson, S., **Novel Bulk Iron Garnets for Magneto-Optic Magnetic Field Sensing**, IEEE Transactions on Magnetics, Vol. 30, No. 6, pp. 4464-4466 (November 1994).

We report measurements of the magneto-optic response function and frequency response for three bulk iron garnet crystals grown by a flux technique. The samples were the product of an intensive effort to develop iron garnet compositions with properties specifically optimized for magnetic field sensing. Sensitivity enhancement was achieved through both bismuth substitution (for increasing the saturation Faraday rotation) and gallium substitution (for reducing the saturation magnetization). One sample exhibited a value of magneto-optic sensitivity of 25° /mT for 1.3-μm light. Frequency response measurements indicate that bismuth substitution actually improves performance (compared to unsubstituted yttrium iron garnet) in contrast with gallium which causes substantial degradation.
[Contact: Merritt N. Deeter, (303) 497-5400]

Rochford, K.B., Day, G.W., and Forman, P.R., **Polarization Dependence of Response Functions in 3 x 3 Sagnac Optical Fiber Current Sensors**, Journal of Lightwave Technology, Vol. 12, No. 8, pp. 1504-1509 (August 1994).

We show theoretically that the response functions of a lossless Sagnac optical fiber current sensor based on a 3 x 3 coupler fundamentally depend on the polarization state of light entering the coupler, even for systems with no linear birefringence. For a lossless, zero-birefringence system the desired response functions, sinusoids separated by 120° phase shifts, are obtained only for circularly polarized input light. The response functions for linearly polarized and depolarized inputs are sinusoids separated by 180° and yield zero-slope small-signal responses; in addition, two outputs are degenerate, so the responses are similar to those observed in 2 x 2 systems. Thus, 3 x 3 Sagnac systems offer no advantage over 2 x 2 systems for linearly polarized input light. The predicted polarization dependence of 3 x 3 Sagnac response functions is experimentally confirmed. This result establishes the need for increased system complexity in 3 x 3 Sagnac current sensors since polarization control optics are required to provide the proper input polarization.
[Contact: Kent B. Rochford, (303) 497-5170]

Rochford, K.B., Rose, A.H., Deeter, M.N., and Day, G.W., **Faraday Effect Current Sensor with Improved Sensitivity-Bandwidth Product**, Optics Letters, Vol. 19, No. 22, pp. 1903-1905, November 15, 1994.

We report a new design for a Faraday effect current sensor based on yttrium iron garnet that has substantially greater bandwidth than previous designs and is much easier to fabricate. The measured sensitivity is 0.7°/A, with a -3dB bandwidth of 500 MHz, which gives an improvement in sensitivity-bandwidth product of approximately 45. A noise-equivalent current of 840 nA/Hz$^{1/2}$ was measured at 1.8 kHz by difference-over-sum processing. The use of turning prisms with phase-preserving coatings greatly simplifies construction, improves electrical isolation, and increases sensitivity through proximity effects.
[Contact: Kent B. Rochford, (303) 497-5170]

Integrated Optics

Released for Publication

Schaafsma, D.T., and Christensen, D.H., **Cross-Sectional Photoluminescence and Its Application to Buried-Layer Semiconductor Structures**.

[See Analysis and Characterization Techniques.]

Veasey, D.L., and Larson, D.R., **An Integrated**

Optical Polarization Diversity Receiver In Glass.

We have successfully demonstrated an integrated optical TE-TM mode discriminator consisting of waveguide polarizers and guided-wave photodetectors. The device consists of a Y-branch waveguide splitter formed by potassium-sodium ion exchange in silicate glass. Hydrogenated amorphous silicon claddings were deposited on each branch of the splitter to act as polarizers. One output cladding was individually trimmed to a thickness which attenuated the TE polarization, while the other cladding was trimmed to attenuate light having TM polarization. The thickness trimming is accomplished using a process of localized plasma etching which allows in-situ extinction optimization by monitoring transmitted light. Extinction ratios of 27 dB were demonstrated for the polarizers with claddings 1.2 mm in length. The integrated receiver was completed with the deposition of metal-semiconductor-metal photodetectors on each of the output waveguide branches following the polarizers. Amorphous silicon claddings were contacted with chrome-gold interdigitated Schottky contacts to form the waveguide detectors.
[Contact: David L. Veasey, (303) 497-5952]

Integrated Optics

Recently Published

Aust, J.A., Malone, K.J., Veasey, D.L., Sanford, N.A., and Roshko, A., **Passively Q-Switched Nd-Doped Waveguide Laser**, Optics Letters, Vol. 19, No. 22, pp. 1849-1851 (November 15, 1994).

A passively Q-switched waveguide laser operating at 1.054 μm has been demonstrated in a Nd-doped phosphate glass. The channel waveguide was fabricated by K-ion exchange from a nitrate melt. Passively Q-switched pulses were achieved by placing a 0.3 optical density acetate sheet containing an organic saturable absorbing dye within the laser cavity. The resulting pulse train consisted of ~25 ns FWHM, 3.04-W peak power pulses. With a 20% transmitting output coupler, cw operation of the laser provided 5.2-mW output power at 1.054 μm for 229-mW-absorbed 794-nm pump power.
[Contact: J. Andrew Aust, (303) 497-3942]

Jinno, M., Schlager, J.B., and Franzen, D.L., **Optical Sampling Using Nondegenerate Four-Wave Mixing in a Semiconductor Laser Amplifier**, Technical Digest of the 1994 Optical Amplifiers and Their Applications Topical Meeting, Breckenridge, Colorado, August 3-5, 1994, Vol. 14, pp. 147-149.

The optical sampling technique, the optical analog of electrical sampling used in electrical sampling oscilloscopes, provides a powerful method for measuring high-speed optical waveforms. Several optical switches have been realized to perform the necessary cross-correlation between sampling and signal pulses. These switches are based on sum frequency generation (SFG) in nonlinear crystals or χ nonlinearities in optical fiber. The optical sampling measurement described here is based on nondegenerate four-wave mixing (NDFWM) in semiconductor laser amplifiers (SLAs). Unlike switches based on nonlinearities in fiber, the SLA offers a compact, environmentally stable medium for efficient cross-correlation signal generation where the necessary condition for phase matching is easily met over a broad range of wavelengths. Unlike optical sampling based on SFG in crystals, no photomultipliers or high-current-gain amplifiers are necessary.

Using NDFWM in an SLA with a tunable, mode-locked erbium-doped fiber laser (T-ML-EDFL) as a probe pulse source, we have achieved optical sampling with picosecond resolution which exceeds the 6-ps temporal resolution of our streak camera. T-ML-EDFLs provide a wavelength-tunable source of high-peak power (>1 W), ultrashort pulses well suited for use as probe pulses in optical sampling, where high-peak powers and not high-repetition rates are required. However, low-probe pulse repetition rates, where the pulse period is much longer than the recovery time of the SLA, allow the amplified spontaneous emission (ASE) in the SLA to build up and become larger than the generated NDFWM signal. We minimize the undesirable effects of this ASE build up by turning on the SLA only when needed. We synchronously gate the SLA with an electrical pulse generated in phase with the sampled signal.
[Contact: John B. Schlager, (303) 497-3542]

Kumar, A., Gallawa, R.L., and Goyal, I.C., **Bend-**

ing-Induced Changes in the Propagation Characteristics of Dual Mode Optical Waveguides, Proceedings of the Conference on Emerging Optoelectronic Technologies, Bangalore, India, July 18-22, 1994, pp. 329-332.

The bending-induced changes in the modal field and power distributions of the first two modes in a bent planar optical waveguide are studied. Unlike the fundamental mode, bending causes the fractional modal power for the second mode to increase in the inner core-half and to decrease in the outer core-half of the waveguide. Interestingly, this leads to a decrease in effective index of the second mode due to bending at sufficiently high *V*-like values.
[Contact: Robert L. Gallawa, (303) 497-3761]

Malone, K.J., **Integrated-Optical Devices in Rare-Earth-Doped Glass**, in Critical Reviews of Optical Science and Technology, Glass Integrated Optics and Optical Fiber Devices, Vol. CR53, S. I. Najafi, Ed. (SPIE, Bellingham, Washington, 1994), pp. 132-156.

Many integrated-optical devices have been demonstrated in rare-earth-doped glasses. They can be used as both laser oscillators and optical amplifiers. These devices have been formed by a number of methods including ion exchange and thin-film deposition. These active integrated-optical devices are expected to be important elements in future optical fiber networks. In this paper, a short overview of these devices is given and some notable achievements are discussed. The fabrication of these components is also included, as well as analytical and diagnostic techniques that can improve performance. A discussion of some current topics in this field concludes this paper.
[Contact: Kevin J. Malone, (303) 497-3289]

Malone, K.J., Veasey, D.L., Sanford, N.A., and Hayden, J.S., **Glasses for Waveguides Lasers**, Proceedings of SPIE (The International Society for Optical Engineering, P.O. Box 10, Bellingham, Washington 98227-0010), Properties and Characteristics of Optical Glass III, Vol. 2287, pp. 75-87 (1994).

Waveguide lasers formed by ion exchange in rare-earth-doped glasses have emerged as an attractive new technology on the threshold of commercial insertion. These devices can be used both as laser oscillators and optical amplifiers. In this article, we review ion exchange and glass composition. We then discuss the performance of ion-exchanged waveguide lasers made in silicate and phosphate glasses.
[Contact: Kevin J. Malone, (303) 497-3289]

Weisshaar, A., Li, J., and Gallawa, R.L., **Efficient Vector Solution for Optical Waveguides Using Galerkin's Method with Hermite-Gauss Basis Functions**, Proceedings of the Conference on Emerging Optoelectronic Technologies, Bangalore, India, July 18-22, 1994, pp. 207-211.

An efficient vector solution for a large class of optical waveguides is presented. The method is based on Galerkin's procedure using Hermite-Gauss basis functions. It is shown that employing Hermite-Gauss basis functions leads to a significant increase in computational efficiency compared to trigonometric basis functions. The accuracy of the method is demonstrated by comparison with the exact solution for the fundamental mode in a circular fiber. In addition to the vector solution, a modified scalar solution which includes a polarization correction is described. Comparison of the modal solutions for optical waveguides with square, rectangular, circular, and elliptical core demonstrate the accuracy of the modified scalar solution.
[Contact: Robert L. Gallawa, (303) 497-3761]

Complex System Testing

Koffman, A.D., Souders, T.M., and Stenbakken, G.N., **NIST Strategies for Reducing Testing Requirements**, Proceedings of the Test and Calibration Symposium, Arlington, Virginia, November 30—December 2, 1994, pp. 267-273.

For the past several years, research has been carried out in the Electricity Division at National Institute of Standards and Technology to reduce the testing requirements for analog and mixed-signal devices. The most significant testing technique to result has been a model-based approach to the testing and calibration of such devices. The model is developed from empirical data, physical information, a priori information, or a combination of the three. Algebraic operations are performed on these

data to create a model. The model approximately spans the vector space within which the device behavior can be described. With this model, the device can be characterized using significantly fewer measurements than is possible with traditional methods. A brief description of the techniques is presented along with a summary of the results achieved in testing analog and mixed-signal devices.
[Contact: Andrew D. Koffman, (301) 975-4518]

Other Signal Topics

Released for Publication

Reeve, G.R., and Friday, D.S., **NIST and the Navy - Past, Present and Future**, to be published in the Proceedings of the Test and Calibration Symposium, American Society of Naval Engineers, Washington, DC, November 30—December 1, 1994.

The National Institute of Standards and Technology, formerly known as the National Bureau of Standards, founded in 1901, has had an historic and fruitful relationship with the Department of Defense, its predecessors, and the three military services, particularly the Navy. In this paper we outline some of the historic support, current collaborations, and what areas of technology may require our support for the Navy of the future.
[Contact: Gerome R. Reeve, (303) 497-3557]

ELECTRICAL SYSTEMS

Power Systems Metrology

Released for Publication

Cookson, A.H., **General Report - CIGRE Session 1994 - Group 15, Insulating Materials**, to be published in the Proceedings of the International Conference on Large High-Voltage Electric Systems, Paris, France, August 29—September 3, 1994.

This is a report of the General Session for Study Committee 15, Insulating Materials, which took place at the CIGRE meeting in Paris, on August 30, 1994. The preferential subjects of new diagnostic techniques and the impact of new materials and systems were discussed. Nine papers had been submitted, and this generated thirty-five formal presentations and over twenty spontaneous discussions. The contributions addressed five key areas: (1) Partial discharge detection and analysis; (2) Gas-insulated systems; (3) Insulation for rotating machines; (4) Polymer materials and high voltage insulators; and (5) Static electrification of transformer oil.
[Contact: Alan H. Cookson, (301) 975-2220]

von Glahn, P.G., and Van Brunt, R.J., **New Measurements of Accelerated Aging Using a Digital Partial Discharge Recording System**.

We describe the design and use of a digital partial discharge (PD) recording system capable of real-time recording of PD pulse trains. The recording system consists of a custom two-channel PD digitizer coupled to a personal computer via a 16-bit parallel interface. The digitizer is under software control with the resulting data being stored in binary files on the computer's hard disk. Since post-test analysis software run on the computer provides the needed stochastic analysis of the data files, the new system offers a unique capability to perform stochastic analysis on non-stationary PD data such as found in aging studies. By way of illustration, we made measurements of the time-varying stochastic behavior of ac-generated PD in point-to-dielectric gaps in air where the insulation material was cast epoxy with aluminum oxide filler, extending the work reported previously. We present sample results demonstrating that the system allows analyses that cannot be made with existing PD stochastic analysis systems and that provide additional insights into the physics of PD.
[Contact: Peter G. von Glahn, (301) 975-2427]

Power Systems Metrology

Recently Published

Van Brunt, R.J., **Physics and Chemistry of Partial Discharge and Corona - Recent Advances and Future Challenges**, IEEE Transactions of Dielectrics and Electrical Insulation, Vol. 1, No. 5, pp. 761-784 (October 1994).

Results of recent research on physical and chemical processes in partial discharge (PD) phenomena are

reviewed. The terminology used to specify different types or modes of PD are discussed in light of a general theory of electrical discharges. The limitations and assumptions inherent to present theoretical models are examined. The influence of memory propagation effects in controlling the stochastic behavior of PD is shown. Examples of experimental results are presented that demonstrate the nonstationary characteristics of PD which can be related to permanent or quasi-permanent discharge-induced modifications (aging) of the site where the PD occur. Recommendations for future research are proposed.
[Contact: Richard J. Van Brunt, (301) 975-2425]

Van Brunt, R.J., and Herron, J.T., **Plasma Chemical Model for Decomposition of SF_6 in a Negative Glow Corona Discharge**, Physica Scripta, Vol. T53, pp. 9-29 (1994).

A zonal plasma chemical model is proposed to account for the observed oxidation and decomposition of sulfur hexafluoride (SF_6) by a negative, point-to-plane glow-type corona discharge in pressurized $SF_6/O_2/H_2O$ gas mixtures. The model yields dependencies of stable neutral oxidation by-products such as SOF_2, SO_2F_2, SOF_4, S_2F_{10}, and SO_2 on time, discharge current, and O_2 and H_2O concentrations which are consistent with measured results. Electron-impact-induced dissociation of SF_6 in the glow region of the discharge is the decomposition rate-controlling process. The relative roles played by different reactions involving neutral free radicals and ions in different zones of the discharge are examined, and in some cases, reaction rate coefficients have been adjusted within reasonable limits to give best fits to observed production rates of various by-products. Problems of uniqueness that arise because of gaps in our knowledge about important processes that should be included in the model are also discussed.
[Contact: Richard J. Van Brunt, (301) 975-2425]

Magnetic Materials and Measurements

Released for Publication

Grishin, A.M., **Interfacial Electron Birefringence: Magnetoresistance in CPP Geometry**.

The theory of giant magnetoresistance is developed for current perpendicular to the plane (CPP) geometry for specular intergrain boundaries. Reflection-transmission (R-T) coefficients are obtained from the boundary conditions of the wave function, the normal components of probability flow, and spin-current continuity. Birefringence of the electron wave takes place at the boundary of crystallographically misaligned grains. Maxwell's equations and Boltzmann's kinetic equation, plus the boundary conditions controlled by R-T coefficients, result in an integral equation for the scalar electric potential and a general formula for interfacial resistance. An analytical form of the R-T coefficients has been found, and a closed expression for interfacial magnetoresistance has been obtained in the case of weak magnetic scattering.
[Contact: Stephen E. Russek, (303) 497-5097]

Hopkins, P.F., Thomson, R.E., Moreland, J., Malhotra, S.S., and Liou, S.H., **Magnetic Force Microscopy Using Fe-(SiO_2) Coated Tips**, to be published in the Digest of the 1995 International Magnetics Conference, San Antonio, Texas, April 18-21, 1995.

Magnetic force microscopy (MFM) is a scanned probe microscopy technique that has been used to achieve high-resolution (typically 50 nm) imaging of the stray magnetic fields above the surface of magnetic materials, including recording media and thin-film recording heads. Although this technique has distinct advantages over other magnetic imaging techniques, the interpretation of the images depends sensitively on the geometry and the magnetic properties of the scanned tip. We report on images obtained with batch micromachined tips coated with thin films of different magnetic materials, and in particular, images obtained with tips coated with granular Fe-(SiO_2) thin films. These films have been shown to have high corrosion and wear resistance, and the magnetic properties can be favorably engineered by controlling the microstructure during the deposition process. In this digest, we show that Fe-(SiO_2)-coated Si_3N_4 cantilevers can be used to obtain high-resolution MFM images with large signal-to-noise ratios.
[Contact: Ruth E. Thomson, (303) 497-3141]

Kim, Y.K., and Sanders, S.C., **Magnetostriction and Giant Magnetoresistance Characteristics of Annealed NiFe/Ag Multilayers**.

We report magnetostriction data for NiFe/Ag multilayer thin films displaying giant magnetoresistance. Magnetostriction and magnetoresistance were measured as a function of annealing temperature for NiFe/Ag samples having different numbers of NiFe/Ag bilayers and Ag spacer thicknesses. Magnetostriction and magnetoresistance varied systematically with annealing temperature in a manner consistent with residual stress reduction and microstructural changes such as grain-boundary diffusion and grain growth. Zero magnetostriction concurrent with high-magnetoresistance ratio (5%) and field sensitivity ($7.5\ \% \cdot kA^{-1} \cdot m = 0.6\ \% \cdot Oe^{-1}$) was observed for an optimal multilayer configuration and annealing temperature. This combination of zero-magnetostriction and high-magnetoresistive response makes the NiFe/Ag multilayer system an attractive candidate for high-performance magnetic recording read-head sensors.
[Contact: Steven D. Sanders, (303) 497-5096]

Kim, Y.K., Sanders, S.C., and Russek, S.E., **Low Magnetostriction in Annealed NiFe/Ag GMR Multilayers**, to be published in the Digest of the 1995 International Magnetics Conference, San Antonio, Texas, April 18-21, 1995.

We have measured the saturation magnetostriction for NiFe/Ag multilayer thin films exhibiting giant magnetoresistance. Zero magnetostriction concurrent with high magnetoresistance ratio ($\Delta R/R = 5\%$) and field sensitivity [7.5%/(kA/m) (0.6%/Oe)] was observed for NiFe/Ag films having an optimal multilayer configuration and annealing temperature. This combination of zero-magnetostriction and high-magnetoresistive response makes the NiFe/Ag multilayer system potentially useful for high-performance magnetic recording read heads.
[Contact: Steven C. Sanders, (303) 497-5096]

Oti, J.O., Russek, S.E., Sanders, S.C., and Cross, R.W., **Models of Discontinuous Giant Magnetoresistance Multilayer Thin Films**.

The correlation between the structural and transport properties for a series of high-quality modulation-doped field-effect transistor (MODFET) structures was made for various growth temperatures. X-ray reflectivity, X-ray diffraction, and magnetotransport measurements were used to assess structural quality and transport parameters. Four samples with growth temperatures in the range 500 °C to 630 °C were examined. The results indicate a correlation exists between the measured electron mobility and the quality of the interface width, as measured from satellite peaks of the buffer layer. Both X-ray and transport results suggest a higher quality structure was obtained at higher growth temperatures.
[Contact: John O. Oti, (303) 497-5557]

Rice, P., and Moreland, J., **Comparison of Magnetic Force Microscopy Techniques**, to be published in the Digest of the 1995 International Magnetics Conference, San Antonio, Texas, April 18-21, 1995.

Magnetic force microscopy is becoming a viable tool for industrial applications. We are presently investigating detection schemes and various new thin-film coatings on micromachined cantilevers that will improve magnetic force microscopy resolution and our ability to quantitatively interpret images. Our future emphasis will be on developing monodomain tips for micromachined cantilevers, since knowing the magnetic state of the tip is key to quantifying magnetic force microscopy images.
[Contact: Paul Rice, (303) 497-3841]

Magnetic Materials and Measurements

Recently Published

Cross, R.W., Russek, S.E., Sanders, S.C., Parker, M.R., Barnard, J.A., and Hossian, S.A., **Size and Self-Field Effects in Giant Magnetoresistive Thin-Film Devices**, IEEE Transactions on Magnetics, Vol. 30, No. 6, pp. 3825-3827 (November 1994).

Giant magnetoresistance was measured as a function of device size for patterned NiCoFe/Cu and NiFe/Ag films. For the quasi-granular NiCoFe/Cu films, the normalized maximum change in resistivity $\Delta p/p$ was 8% for most of the samples. For the NiFe/Ag films, anti-parallel alignment was achieved through magnetostatic coupling, not exchange fields, with a $\Delta p/p$ of 4.5%. The films were patterned into stripes with Au current leads for size-effect measurements. The height of the stripes

varied from 0.5 to 16 μm, and the track width varied from 1 to 16 μm. Discrete switching events and anomalous low-field dips in the response were observed for both materials for small device sizes. Self-field and heating effects due to the applied current were investigated for the NiFeCo/Cu films. The effect of the self-field produced by the applied current was separated from the thermal contribution and was found to reduce the response by over 32% for a current density of 10^7 A/cm^2.
[Contact: R. William Cross, (303) 497-5300]

Rice, P., Hallett, B., and Moreland, J., **Comparison of Magnetic Fields of Thin-Film Heads and Their Corresponding Bit Patterns Using Magnetic Force Microscopy**, IEEE Transactions on Magnetics, Vol. 30, No. 6, pp. 4248-4250 (November 1994).

We have used dc-mode magnetic force microscopy to image the magnetic fringing fields of several thin-film heads and the bit patterns written with these heads. The images were taken with Si_3N_4 tips coated with 10-nm Fe and 5-nm Au. The heads and disks are typical industry standards. The heads had a variety of pole piece configurations. A large track separation was used so that the erase bands could be thoroughly studied. We were surprised to discover magnetic fields that correspond to layers in the alumina overcoat near the pole pieces. The magnetic force microscope images of the bit pattern show a definite twist at the track edge that points toward the trailing pole piece. We also observed disk magnetization patterns that remained after an ac erase procedure.
[Contact: Paul Rice, (303) 497-3841]

Rice, P., and Moreland, J., **Flexible-Diaphragm Force Microscope**, Journal of Vacuum Science and Technology B, Vol. 12, No. 4, pp. 2465-2466 (July/August 1994).

A flexible polyimide diaphragm was used in place of the usual cantilever for atomic force microscopy. Images of hard disk surface features are presented demonstrating the practicality of the method.
[Contact: Paul Rice, (303) 497-3841]

Wadas, A., Rice, P., and Moreland, J., **Recent Results in Magnetic Force Microscopy**, Applied Physics A, Vol. 59, pp. 63-67 (1994).

We present domain wall images obtained by using Magnetic Force Microscopy (MFM) on magnetic samples like: double layer of permalloy alloy, magnetic hard disk, $BaFe_{12}O_{19}$ single crystal and YGdTmGa/YSmTmGa magnetic garnet. We have imaged topography and magnetic forces of the same area. The Fe double- and single-layer thin film tips have been prepared to achieve high-sensitivity (10^{-12} N) and high-resolution of MFM.
[Contact: Paul Rice, (303) 497-3841]

Superconductors

Released for Publication

Bray, S.L., Ekin, J.W., Waltman, D.J., and Superczynski, M.J., **Quench-Energy and Fatigue Degradation Properties of Al- and Cu-Stabilized NbTi Epoxy-Impregnated Superconductor Coils**.

In comparative measurements of small-scale epoxy-impregnated Cu-stabilized and Al-Cu-stabilized NbTi test coils at 4 K and 5 T, the heat energy required to quench the Al-Cu-stabilized coil was 4 to 12 times greater than for the Cu-stabilized coil, depending on the relative operating current. Also, the coils' stabilizer resistivity (ρ) was measured as a function of mechanical fatigue to test for strain-induced degradation. The ρ of the Cu-stabilized coil is relatively unaffected by fatigue, while that of the Al-stabilized coil increases with fatigue. However, in these coils, having a typical stabilizer:superconductor ratio of 4:1, the degradation of the Al-Cu-stabilized coil begins to saturate after several hundred fatigue cycles, and, after 2000 fatigue cycles to 0.2% strain, the ρ of the Al-Cu-stabilized coil is still 2.6 times lower than the ρ of the Cu-stabilized coil. Furthermore, after annealing the Al-Cu-stabilized coil at room temperature for 48 h, the ρ degradation was reduced by 76%. Thus, the use of Al-Cu-stabilizer may offer substantial improvements in magnet stability even where the magnet is subjected to fatigue degradation from repeatedly energizing the magnet.
[Contact: Steven L. Bray, (303) 497-5631]

Cooley, L.D., and Grishin, A.M., **Pinch Effect in Commensurate Vortex-Pin Lattices**.

The critical state in a superconductor with periodic

pins is found to be an analog of the pinch effect, known in plasma physics. It forms a terrace structure around the average flux density gradient, causing stratification of the transport current into the terrace edges where the flux density gradient is large. Thus, regions of extremely high current interlace with regions of near zero current. The elastic repulsion between vortices and the matching of the fluxon lattice to the pin lattice act against the average flux density gradient, so that the balance determines the terrace height and width. Wide terraces occur when the pinning force is high and the fluxon lattice is stiff. The appearance of each new terrace inside the superconductor gives rise to oscillations in the magnetization as a function of field, as seen in recent experiments. The addition of one flux quantum threading the pin unit cell determines the periodicity of the peaks; thus the oscillations represent a quantum effect.
[Contact: Lance D. Cooley, (303) 497-7747]

Ekin, J.W., Bray, S.L., Bergren, N.F., and Tenbrink, J., **Enhanced Strain and Stress Tolerance of Bi-2212 Superconductors with AgNiMg Sheathing**.

The axial strain degradation of the critical current of $Bi_2Sr_2Ca_1Cu_2O_{8+x}$ (Bi-2212) superconductors has been measured on Ag- and AgNiMg-sheathed wires that were cooled in a force-free manner without additional sample holder strain. A direct comparison between Ag- and AgNiMg-sheathed Bi2212 conductors having the same number of filaments, matrix:superconductor ratio, and overall wire diameter shows that the irreversible strain limit (where the critical current is degraded 10% from its initial value) is significantly higher (~0.7%) in the AgNiMg-sheathed conductors than in the Ag-sheathed conductors (~0.4%). At lower criteria levels for e_{irrev} (5% or 2%), the difference is less, suggesting that cracking starts at a relatively low strain (0.4% to 0.5%) even in the AgNiMg-sheathed materials. The higher yield strength of AgNiMg compared with Ag may explain both the increased strain tolerance and lower degradation rate in the AgNiMg-sheathed wires. We also observe that, for both types of sheathing materials, the conductors with the finest filament diameters have the highest J_c values. At the same time, however, they also have the lowest strain limits for irreversible J_c damage. We suggest that both effects are a result of the greater amount of textured material in the conductors having the largest amount of Bi-2212/Ag interface area. Finally, we suggest that the discrepancy between the observed small prestrain and large differential thermal contraction in Bi-2212 composites may be due to yielding of the Bi-2212 material, rather than the Ag sheathing.
[Contact: John W. Ekin, (303) 5448]

Goodrich, L.F., Wiejaczka, J.A., Srivastava, A.N., Stauffer, T.C., and Medina, L.T., **First VAMAS USA Interlaboratory Comparison of High Temperature Superconductor Critical Current Measurements**.

We conducted an interlaboratory comparison of critical current (I_c) measurements with Bi-based oxide tape (2223) high-temperature superconductors (HTS). This study includes measurements from six participating U.S. laboratories, with NIST as the central, organizing laboratory. A number of specimens were prepared with different degrees of instrumentation to isolate sources of variability. Most of the specimens were pre-measured by NIST to reduce uncertainties due to specimen inhomogeneity. Different specimen routing patterns, among the laboratories, were implemented to isolate sources of variability due to the specimen's measurement history. This study is similar to other VAMAS intercomparisons being performed in Japan and Europe and is the first internationally cooperative interlaboratory comparison of HTS I_c measurements. These are the first steps towards developing standard measurement procedures for HTS.
[Contact: Loren F. Goodrich, (303) 497-3143]

Goodrich, L.F., Wiejaczka, J.A., Srivastava, A.N., Stauffer, T.C., and Medina, L.T., **USA Interlaboratory Comparison of Superconductor Simulator Critical Current Measurements**.

An interlaboratory comparison of critical current (I_c) measurements was conducted on the superconductor simulator which is an electronic circuit that emulates the extremely nonlinear voltage-current characteristic of a superconductor. These simulators are high-precision instruments, and are useful for establishing the integrity of part of a superconductor measurement system. This study includes measurements from participating U.S. laboratories, with NIST as the central organizing

laboratory. This effort was designed to determine the sources of uncertainty in I_c measurements due to uncertainties in the measurement apparatus, technique, or the analysis system. These results could significantly benefit superconductor measurement applications that require high-precision quality assurance.
[Contact: Loren F. Goodrich, (303) 497-3143]

Superconductors

Recently Published

Goodrich, L.F., and Srivastava, A.N., **A Simple and Repeatable Technique for Measuring the Critical Current of Nb_3Sn Wires**, Proceedings of the 7th International Workshop on Critical Currents in Superconductors, Alpbach, Austria, January 24-27, 1994, pp. 609-612.

We evaluated an alternate approach for measuring the critical current (I_c) of Nb_3Sn wire which uses a standard mandrel geometry and apparatus interface. Preliminary data indicate that the tension in the conductor before reaction and measurement may affect the repeatability. We also show preliminary summary statistics for measurements of conductors performed by five U.S. laboratories. The reaction and measurement mandrel used was fabricated using a Ti_6Al_4V alloy. This high-temperature alloy was used to avoid transferring the specimen between mandrels, thus reducing the likelihood of inadvertent mechanical damage of the specimen. Besides this advantage, these holders are inexpensive and nonmagnetic, and have a low thermal expansion and a high electrical resistivity (147 $\mu\Omega$·cm at 4 K). Using the same mandrel for reaction and measurement improves the quality assurance of the I_c measurement for database creation and acceptance testing for large-scale applications such as ITER (International Thermonuclear Experimental Reactor). The U.S. ITER Home Team adopted this approach in a recent test because it was expected to be easily implemented and yield consistent results.
[Contact: Loren F. Goodrich, (303) 497-3143]

Goodrich, L.F., Wiejaczka, J.A., Srivastava, A.N., and Stauffer, T.C., **Superconductor Critical Current Measurement Standards For Fusion Applications**, NISTIR 5027 (November 1994).

This report describes research conducted to help establish a standard critical measurement technique for Nb_3Sn wires that may be used in fusion applications. The main part of this report is a detailed presentation of results of the first International Thermonuclear Experimental Reactor international laboratory comparison of Nb_3Sn critical current measurements. A common procedure and a common reaction and measurement mandrel was used by U.S. laboratories in this comparison, whereas there was no common procedure followed by other international laboratories. The largest difference in I_c measurements of two laboratories that did not use a common procedure was 23%. The largest difference in I_c measurements of two laboratories that did use a common procedure was 6.5%. There may still be room for improvement, but this indicates the strong need for a common detailed procedure. Results on the homogeneity of one of the Nb_3Sn wires used in this study and a commentary on creating a Nb_3Sn Reference Wire are also presented.
[Contact: Loren F. Goodrich, (303) 497-3143]

Wada, H., Walters, C.R., Goodrich, L.F., and Tachikawa, K., **VAMAS Intercomparison of Critical Current Measurements on Nb_3Sn Superconductors: a summary report**, Cryogenics, Vol. 34, No. 11, pp. 899-908 (1994).

This paper is a summary of an international collaboration endorsed by VAMAS to study problems associated with critical current measurements in Nb_3Sn superconductors and provide guidelines for a standard measurement. Two series of critical current measurements were implemented. In the first series, three different sample conductors were used and participants made measurements using their own techniques. As a result, coefficients of variation for these samples at 12 T turned out to be 8 to 29.9%. A major source of these variations was attributed to strain sensitivity of the Nb_3Sn conductors. Thus, the second series of measurements were done on one sample conductor and under specified measurement conditions, particularly in terms of specimen strain. The coefficient of variation decreased to 2.2%, which is regarded as a reasonable base for future establishment of an international standard measurement method.

[Contact: Loren F. Goodrich, (303) 497-3143]

ELECTROMAGNETIC INTERFERENCE

Radiated EMI

Released for Publication

Camell, D.G., and Ma, M.T., **Assessment of Particular Measurement Data by a Linear Transfer Function Technique**, to be published as NIST Technical Note 1372.

The newly developed theory for predicting the response of a linear system to an electromagnetic pulse, based only on the measured continuous-wave (cw) magnitude, is applied to a particular system as a case study. The problem being addressed is concerned with possible electromagnetic interferences at a sensitive part of a torpedo. The measured magnitude representing the system's transfer function is deduced first from the measured response at this sensitive point to a known cw source, supplied by the Naval Surface Warfare Center. We then derive an analytic expression for the magnitude square of the transfer function to approximate the measured data, and obtain a system transfer function in terms of the complex frequency, from which we predict the system cw phase characteristics and its multiple solutions due to a given impulse source.
[Contact: Dennis G. Camell, (303) 497-3214]

Hill, David A., **Spatial Correlation Function for Fields in a Reverberation Chamber**.

In a recent paper, we described random fields in a reverberation chamber by an integral representation of plane waves over all real angles. A physical interpretation of the random field in a reverberation chamber is that each member of the ensemble corresponds to a different stirrer (tuner) position. The plane-wave spectrum representation has been found useful for providing a mathematical description for the response of a receiving antenna or other test object in a reverberation chamber and for calculating the quality factor (Q) for reverberation chambers of arbitrary geometries. The purpose of this correspondence is to show that the plane-wave spectrum representation can also be used to provide a simple derivation for the spatial correlation function of the fields.
[Contact: David A. Hill, (303) 497-3472]

Radiated EMI

Recently Published

Hill, D.A., **Electronic Mode Stirring for Reverberation Chambers**, IEEE Transactions on Electromagnetic Compatibility, Vol. 36, No. 4, pp. 294-299 (November 1994).

A modal analysis and a uniform-field approximation are presented for the fields in an idealized two-dimensional, rectangular cavity excited by an electric line source. The model is used to evaluate the effectiveness of frequency stirring, an alternative to mechanical stirring in reverberation chamber immunity measurements. Numerical results indicate that good field uniformity (standard deviation less than 1 dB) can be obtained with a bandwidth of 10 MHz at a center frequency of 4 GHz. The bandwidth requirement is determined primarily by the number of modes excited, and higher frequencies can achieve the same field uniformity with a smaller bandwidth because of the higher mode density. Cavity excitation by two single-frequency sources is also analyzed.
[Contact: David A. Hill, (303) 497-3472]

Hill, D.A., Cavcey, K.H., and Johnk, R., **Crosstalk Between Microstrip Transmission Lines**, IEEE Transactions on Electromagnetic Compatibility, Vol. 36, No. 4, pp. 314-321 (November 1994). [Also published as NISTIR 5015 (December 1993).]

Methods for prediction of crosstalk between microstrip transmission lines are reviewed and simplified for the weak coupling case. Classical coupled transmission line theory is used for uniform lines, and potential and induced electromagnetic field methods are used for crosstalk between nonuniform lines. It is shown that the potential method is equivalent to classical coupled transmission line theory for the case of uniform lines. An experiment was performed for uniform coupled microstrip lines for frequencies from 50 MHz to 5 GHz, and good agreement between theory and measurement was obtained for both near- and far-end crosstalk.

[Contact: David A. Hill, (303) 497-3472]

Hill, D.A., Ma, M.T., Ondrejka, A.R., Riddle, B.F., Crawford, M.L., and Johnk, R., **Aperture Excitation of Electrically Large, Lossy Cavities**, IEEE Transactions on Electromagnetic Compatibility, Vol. 36, No. 3, pp. 169-178 (August 1994). [A more extensive treatment was published as NIST Technical Note 1361 (September 1993).]

We present a theory based on power balance for aperture excitation of electrically large, lossy cavities. The theory yields expressions for shielding effectiveness, cavity Q, and cavity time constant. In shielding effectiveness calculations, the incident field can be either a single plane wave or a uniformly random field to model reverberation chamber or random field illumination. The Q theory includes wall loss, absorption by lossy objects within the cavity, aperture leakage, and power received by antennas within the cavity. Extensive measurements of shielding effectiveness, cavity Q, and cavity time constant were made on a rectangular cavity, and good agreement with theory was obtained for frequencies from 1 to 18 GHz.
[Contact: David A. Hill, (303) 497-3472]

ADDITIONAL INFORMATION

Lists of Publications

Smith, A.J., **Metrology for Electromagnetic Technology: A Bibliography of NIST Publications**, NISTIR 5029 (September 1994).

This bibliography lists the publications of the personnel of the Electromagnetic Technology Division of NIST during the period from January 1970 through publication of this report. A few earlier references that are directly related to the present work of the Division are also included.
[Contact: Annie Smith, (303) 497-3678]

Lyons, R.M., and Gibson, K.A., **A Bibliography of the NIST Electromagnetic Fields Division Publications**, NISTIR 5028 (September 1994).

This bibliography lists publications by the staff of the National Institute of Standards and Technology's Electromagnetic Fields Division for the period from January 1970 through July 1993. Selected earlier publications from the Division's predecessor organizations are included.
[Contact: Kathryn A. Gibson, (303) 497-3132]

Meiselman, B., **Electrical and Electronic Metrology: A Bibliography of NIST Electricity Division's Publications, NIST List of Publications 94** (January 1994).

This bibliography covers publications of the Electricity Division, Electronics and Electrical Engineering, Laboratory, NIST, and of its predecessor sections for the period January 1968 to December 1993. A brief description of the Division's technical program is given in the introduction.
[Contact: Katherine H. Magruder, (301) 975-2401]

Walters, E.J., **Semiconductor Measurement Technology, 1990-1993, NIST List of Publications 103** (January 1994).

The bibliography provides information on technology transfer in the field of microelectronics at NIST for the calendar years 1990 through 1993. Publications from groups specializing in semiconductor electronics are included, along with NIST-wide research now coordinated by the NIST Office of Microelectronics Programs which was established in 1991. Indices by topic area and by author are provided. Earlier reports of work performed during the period from 1962 through December 1989 are provided in NIST List of Publications 72.
[Contact: E. Jane Walters, (301) 975-2050]

Availability of *Measurements for Competitiveness in Electronics* [First Edition], NISTIR 4583 (April 1993).

This document is the successor to NISTIR 90-4260, *Emerging Technologies in Electronics ...and their Measurement Needs* [Second Edition]. The new *Measurements for Competitiveness in Electronics* identifies the measurement needs that are most critical to U.S. competitiveness, that would have the highest economic impact if met, and that are the most difficult for the broad range of individual companies to address. The document has two primary purposes: (1) to show the close relationship between U.S. measurement infrastructure and U.S. competitiveness, and show why improved measurement capability offers such high economic leverage and (2) to provide a consensus on the

principal measurement needs affecting U.S. competitiveness, as the basis for an *action plan* to meet those needs and to improve U.S. competitiveness.

Copies of this document are available as Order No. PB93-160588 from the National Technical Information Service, 5285 Port Royal Road, Springfield, VA 22161, at (800) 553-6847 or (703) 487-4650.

Abstract -- Measurements are used to determine the values of hundreds of important quantities in the electronics industry. Representative quantities are the widths of the interconnections within semiconductor integrated circuits, the attenuation of lightwaves in optical fibers, and the signal power from microwave satellite antennas. Measurement capability is a fundamental tool used to build the nation's high-technology products. As such, it is part of the national infrastructure for the realization of these products.

Measurement capability is critical to research and development, manufacturing, marketplace entry, and after-sales support of products. Thus, measurement capability affects the performance, quality, reliability, and cost of products. The result of this pervasive impact is that the level of U.S. measurement capability places an upper limit on the competitiveness of U.S. products.

At present, U.S. industry is experiencing a major shortfall in the measurement capability needed for competitiveness in electronic products. This document identifies the measurement needs that are most critical to U.S. competitiveness, that would have the highest economic impact if met, and that are the most difficult for the broad range of individual companies to address. The measurement needs are reviewed for nine important fields of electronics, including semiconductors, magnetics, superconductors, microwaves, lasers, optical-fiber communications, optical-fiber sensors, video, and electromagnetic compatibility. These fields of electronics underlie more than $300 billion of electronic and electrical products manufactured in the U.S. each year.

This assessment provides the framework for an action plan to correct the shortfall in U.S. measurement capability in electronics and to advance U.S. competitiveness.

Guide -- The compiler of the document provided an introductory guide to its organization and content. Because EEEL believes that a number of *TPB* readers will be interested in the information presented in the various chapters, the contents of this guide are reproduced below (page numbers of chapter summaries are included to provide a measure of the extent of the treatment):

This document contains 12 chapters, divided into two groups. The first three chapters are introductory in nature and are relevant to all of the following chapters. The remaining nine chapters address individual fields of electronic technology. Each chapter begins with a two-page summary that provides ready access to the major points made in the chapter. These short summaries are found on the pages identified below. By selecting from these summaries, you can quickly access information on the subjects of most interest to you.

Introductory Information -- Chapter 1, Role of Measurements in Competitiveness (page 3); Chapter 2, NIST's Role in Measurements (page 21); Chapter 3, Overview of U.S. Electronics and Electrical-Equipment Industries (page 31).

These three chapters introduce the subject of measurements and provide an overview of the products of the U.S. electronics and electrical-equipment industries.

Chapter 1, **Role of Measurements in Competitiveness**, shows why measurements are a fundamental part of the infrastructure of the nation. Chapter 1 also sets measurements in the context of the many other important factors that affect competitiveness.

Chapter 2, **NIST's Role in Measurements**, indicates the circumstances under which Government assistance to industry in the development of measurement capability is appropriate in pursuit of a strengthened national economy.

Chapter 3, **Overview of U.S. Electronics and Electrical-Equipment Industries**, introduces these industries through an overview of their major product lines. This chapter shows the various ways in which the products of these industries are commonly classified and how those classifications

relate to the structure of this document.

Fields of Technology -- Chapter 4, Semiconductors (page 53); Chapter 5, Magnetics (page 95); Chapter 6, Superconductors (page 129); Chapter 7, Microwaves (page 147); Chapter 8, Lasers (page 183); Chapter 9, Optical-Fiber Communications (page 217); Chapter 10, Optical-Fiber Sensors (page 303); Chapter 11, Video (page 339); Chapter 12, Electromagnetic Compatibility (page 381).

Each of these chapters contains four basic types of information:

Technology Review: The field of technology is reviewed to highlight and explain the special capabilities that make the technology important. This review introduces the technical concepts that are necessary for understanding the sections that follow.

World Markets and U.S. Competitiveness: The economic significance of the field of technology is highlighted through use of national and international market data for major products that employ the technology. Available information on the U.S. competitiveness is described.

Goals of U.S. Industry for Competitiveness: The goals that U.S. industry is pursuing to improve its competitiveness are discussed so that they can be related to requirements for new measurement capability supportive of the goals.

Measurement Needs: The new measurement capability that U.S. industry will need to enable it to achieve its goals is described. This discussion emphasizes measurement capability that is needed widely in U.S. industry, that will have high economic impact if provided, and that is beyond the resources of the broad range of individual U.S. companies to provide.

[While the assessment of measurement needs in this document is wide ranging, not every field of technology important to the electronic and electrical-equipment industries has been covered. NIST plans to expand this assessment in future editions to include additional fields.]

The order in which chapters appear is intentional: the technologies on which most other technologies depend are introduced first. Thus, the chapter on semiconductors appears first because most electronic technologies depend on semiconductor materials. In contrast, the chapter on video is located near the end because it depends on nearly every other technology discussed earlier.

Chapters 4, 5, and 6 of this document describe the measurement needs arising from three important materials technologies that underlie current and emerging electronic and electrical products. These chapters also describe the measurement needs of components and equipment based on these materials and not discussed separately in other chapters.

Chapter 4, **Semiconductors**, addresses both silicon and compound semiconductors and their use in components, including individual (discrete) electronic and optoelectronic devices and integrated circuits. Semiconductor components are central to all modern electronic products from consumer products to supercomputers.

Chapter 5, **Magnetics**, focuses on both magnetic materials and the components made from them. Magnetic materials are second in importance only to semiconductor materials for electronic products and play a central role in electrical products. This chapter also addresses the measurement needs of selected equipment critically dependent on magnetic materials, including magnetic information storage equipment, electrical power transformers, and others.

Chapter 6, **Superconductors**, examines superconductor materials and addresses both present and emerging applications of these materials in electronic and electrical products.

Chapters 7 through 11 describe the measurement needs associated with selected technologies of importance to U.S. competitiveness for current and emerging products.

Chapter 7, **Microwaves**, describes the highest-information-capacity radio technology. Microwave electronics provide the basis for modern and emerging wireless communications systems and radar systems. Included are new personal communications services with both local and worldwide

access, intelligent vehicle-highway systems, and advanced audio and video broadcasting systems, among others.

Chapter 8, **Lasers**, addressed the single most important component for emerging lightwave systems used for manufacturing, medicine, communications, printing, environmental sensing, and many other applications.

Chapter 9, **Optical-Fiber Communications**, describes the highest-information-capacity cable technology. It provides the basis for national and international information highways of unprecedented performance and broad economic impact. Optical-fiber systems will be linked with microwave systems to interconnect mobile and portable users and to backup cable systems.

Chapter 10, **Optical-Fiber Sensors**, focuses on an emerging class of sensors that offers outstanding performance for a broad spectrum of applications in manufacturing, aerospace, medicine, electrical power, and other areas.

Chapter 11, **Video**, emphasizes advanced, high-performance systems, such as high-definition television, which offer, for the first time, simultaneous access to high-resolution, smooth motion, and great color depth. The chapter notes the potential of full-power implementations of video technology in interactive networked environments. The chapter contains a special focus on flat-panel displays.

Chapter 12, **Electromagnetic Compatibility**, describes the special challenges that the U.S. faces in maintaining electromagnetic compatibility among the many new products of electronic and electrical technologies. Such compatibility is essential if the full potential of all of the above technologies is to be realized without debilitating mutual interference.

Appendices -- The three appendices provide definitions of the U.S. electronics and electrical-equipment industries. These definitions were used in preparing much of the economic information in the report.

Appendix 1 describes the Standard Industrial Classification System that the U.S. Government uses for collecting data about U.S. industry. This appendix also lists publications in which the U.S. Government reports data on U.S. shipments.

Appendix 2 provides a definition of the U.S. electronics industry in terms of the Standard Industrial Classification System.

Appendix 3 provides a definition of the U.S. electrical-equipment industry in terms of the Standard Industrial Classification System.

1995 Calendar of Events

March 20-22, 1995 (Research Triangle Park, North Carolina)

Third International Workshop on the Measurement and Characterization of Ultra-Shallow Doping Profiles in Semiconductors. Sponsored by the American Vacuum Society, Intel, MCNC, SEMATECH, and the NIST Office of Microelectronics Programs, this Workshop will provide a forum for a thorough discussion and evaluation of various one- and two-dimensional techniques available for the measurement of ultra-shallow doping profiles in semiconductors. Topics to be discussed are process model verification, sputter depth profiling, spreading resistance profiling, and microscopy for junction profiling and interface characterization.
[Contact: James R. Ehrstein, (301) 975-2060]

April 27, 1995 (Wakefield, Massachusetts)

Ion Implant Users Group Meeting. Sponsored by NIST, the Spring Meeting of the Ion Implant Users Group will present discussions on Particles II and Buried Layers and Ion Implantation. Wednesday, April 26, has been set aside for visiting the MIT Microtechnology Laboratory, the Lincoln Lab New Class 10 Fabrication Facility, and the Implant Sciences Facility.
[Contact: John Albers, (301) 975-2075]

October 8-12, 1995 (Orlando, Florida)

Special Session on Model Validation, 1995 IEEE-IAS Annual Meeting. The Power Electronics Devices and Components Committee of the IEEE Industry Applications Society in cooperation with the NIST Working Group on Model Validation will hold

a special session on model validation. This session is being introduced to reflect the growing needs and interest in establishing procedures for the comprehensive evaluation of circuit simulator models. Topics of interest include: characterization procedures that could be applied for evaluation of models, methods for identifying and implementing model validation procedures, and the application of validation procedures in comparing specific models. [Contact: Allen R. Hefner, (301) 975-2071]

EEEL Sponsors

National Institute of Standards and Technology
Executive Office of the President
U.S. Air Force
  Hanscom Air Force Base; Newark Air Force Base; CCG-Strategic Defense Command; CCG-Systems Command; Wright Patterson
U.S. Army
  Fort Belvoir; Redstone Arsenal; Combined Army/Navy/Air Force (CCG)
Department of Defense
  Advanced Research Projects Agency; Defense Nuclear Agency; National Security Agency
Department of Energy
  Building Energy R&D; Energy Systems Research; Fusion Energy; Basic Energy Sciences;
Department of Justice
  Law Enforcement Assistance Administration; Federal Bureau of Investigation
U.S. Navy
  CCG, Seal Beach; Office of Naval Research; Naval Surface Warfare Center
National Aeronautics and Space Administration
  NASA Headquarters
Department of Transportation
  National Highway Traffic Safety Administration;
Central Intelligence Agency
MIMIC Consortium
Nuclear Regulatory Commission
Department of Health and Human Services
  National Institutes of Health
Various Federal Government Agencies

NIST SILICON RESISTIVITY SRMs

In response to needs of the semiconductor industry, NIST's Semiconductor Electronics Division provides silicon bulk resistivity Standard Reference Materials (SRMs) through the NIST Standard Reference Materials Program. A new class of resistivity SRMs is being introduced to respond better to users' requirements.

The first NIST (then NBS) resistivity SRMs were fabricated from crystal 50 mm (2 in) in diameter. These wafers represented various combinations of crystal growth process, crystallographic orientation, and doping, each combination chosen to give the best expected wafer uniformity for a given resistivity level. Each wafer in every set was individually measured and certified. Some of these sets are still available until the supply is exhausted (see table).

The Division is now certifying single-wafer resistivity standards at approximately the same resistivity values as were available in the earlier sets. These new SRMs are fabricated from crystal 100 mm in diameter, intended to provide improved compatibility with newer end-use instrumentation. In response to user comments, the new SRMs will be more uniform in both thickness and resistivity, will have reduced uncertainty of certified value due to use of an improved certification procedure using a four-point probe, and will be measured and certified at additional measurement sites for better characterization of wafer uniformity at its core. The additional measurements needed to qualify the improved SRMs will make them more expensive on a per-wafer basis than the earlier sets.

NIST SILICON BULK RESISTIVITY STANDARD REFERENCE MATERIALS

DATE UPDATED: 10 MARCH 1995

Note: Problems in producing and certifying new SRMs have resulted in substantial delays. The first to become available, for 10 and 180 ohm · cm, are not likely to be ready until 1995.

NOMINAL RESISTIVITY (ohm · cm)	OLD SRMs	AVAILABILITY	NEW SRMs	ANTICIPATED AVAILABILITY
0.01	1523 (one of set of two wafers)	limited supply	2541	to be announced
0.1	1521 (one of set of two wafers)	limited supply	2542	to be announced
1	1523 (one of set of two wafers)	limited supply	2543	to be announced
10	1521 (one of set of two wafers)	limited supply	2544	to be announced
25	1522	set of three wafers no longer available	2545	to be announced
75	1522		2546 (100)	to be announced
180	1522		2547 (200)	to be announced

The above table will be updated in future issues to reflect changes in availability. Every effort will be made to provide accurate statements of availability; NIST sells SRMS on an as-available basis. For technical information, contact James R. Ehrstein, (301) 975-2060; for ordering information, call the Standard Reference Materials Program Domestic Sales Office: (301) 975-6776.

The National Institute of Standards and Technology

NIST Standard Reference Materials (SRMs) are used by thousands of companies to calibrate their equipment

NIST photomask SRMs help reduce linewidth measurement errors by a factor of 10 and save manufacturers over $30 million annually

NIST research in electromigration is saving manufacturers over $26 million and has contributed to a new thrust in building-in reliability

NIST research improved production yield of high reliability devices by factors of 2 to 35

NIST developed a tester that characterizes the breakdown of semiconductor power devices without destroying them

NIST is developing test structures and test methods for nanometer overlay metrology

NIST is developing new optical measurement tools for advanced semiconductor manufacturing

NIST research works.

Find out how NIST can help you.
See us at SEMICON/West '95
July 11-13, 1995, San Francisco, Calif.

Hall 4, Booth 6547
MOSCONE CENTER

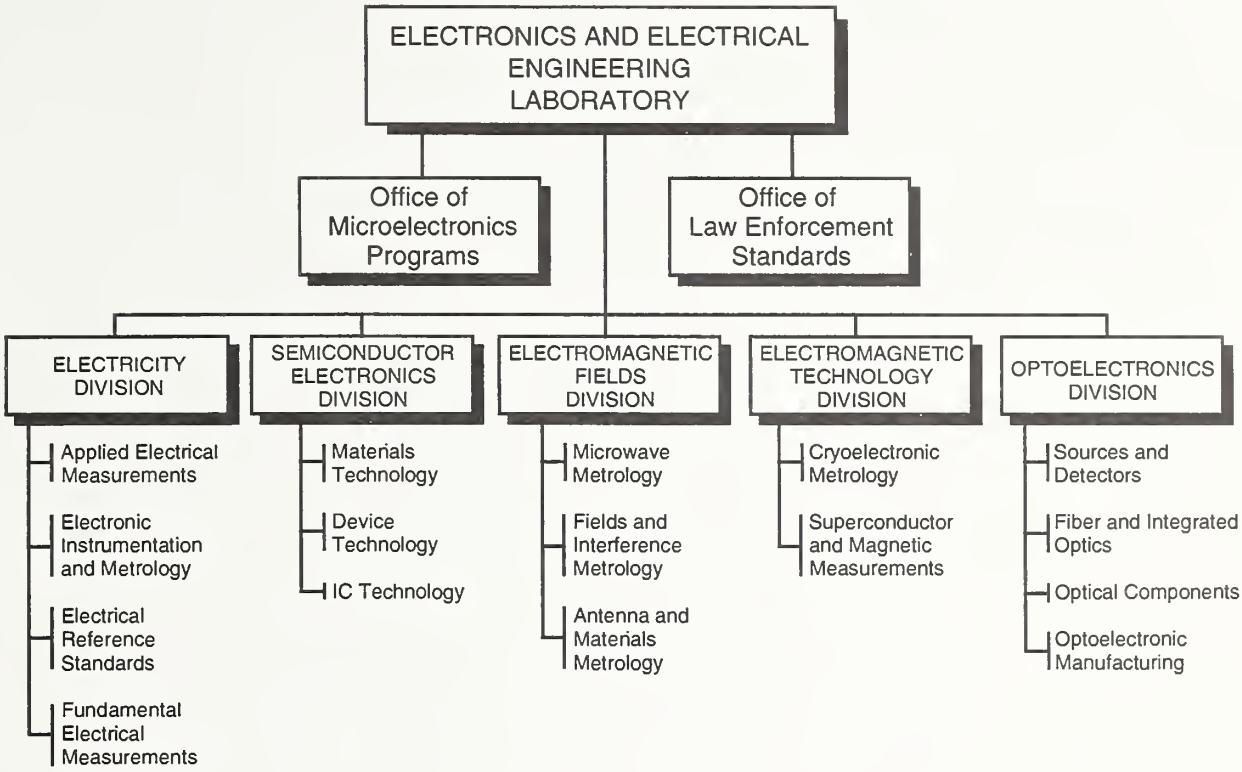

KEY CONTACTS

Laboratory Headquarters (810)	Director, Judson C. French (301) 975-2220
	Deputy Director, Robert E. Hebner (301) 975-2220
	Associate Director, Alan H. Cookson (301) 975-2220
Office of Microelectronics Programs	Director, Robert I. Scace (301) 975-4400
Office of Law Enforcement Standards	Director, Kathleen M. Higgins (301) 975-2757
Electricity Division (811)	Acting Chief, William E. Anderson (301) 975-2400
Semiconductor Electronics Division (812)	Chief, Frank F. Oettinger (301) 975-2054
Electromagnetic Fields Division (813)	Chief, Allen C. Newell (303) 497-3131
Electromagnetic Technology Division (814)	Acting Chief, Richard E. Harris (303) 497-3776
Optoelectronics Division (815)	Chief, Gordon W. Day (303) 497-5204

INFORMATION:

For additional information on the Electronics and Electrical Engineering Laboratory, write or call:

Electronics and Electrical Engineering Laboratory
National Institute of Standards and Technology
Metrology Building, Room B-358
Gaithersburg, MD 20899
Telephone: (301) 975-2220

U.S. DEPARTMENT OF COMMERCE
NATIONAL INSTITUTE OF STANDARDS AND TECHNOLOGY
GAITHERSBURG, MD 20899-0001

OFFICIAL BUSINESS
PENALTY FOR PRIVATE USE, $300

DO NOT FORWARD
ADDRESS CORRECTION REQUESTED
RETURN POSTAGE GUARANTEED

BULK RATE
POSTAGE & FEES PAID
NIST
PERMIT No. G195